https://doi.org/10.5194/egusphere-2023-117
Preprint. Discussion started: 2 March 2023

Introducing a Comprehensive Set of Stratospheric Aerosol Injection Strategies

Yan Zhang[1], Douglas G. MacMartin[1], Daniele Visioni[1], Ewa Bednarz[1,2,3], and Ben Kravitz[4,5]

[1]Sibley School of Mechanical and Aerospace Engineering, Cornell University, Ithaca, NY, USA
[2]CIRES, University of Colorado Boulder, Boulder, CO, USA
[3]NOAA Chemical Sciences Laboratory, Boulder, CO, USA
[4]Department of Earth and Atmospheric Science, Indiana University, Bloomington, IN, USA
[5]Atmospheric Sciences and Global Change Division, Pacific Northwest National Laboratory, Richland, WA, USA

Correspondence: Yan Zhang (yz2545@cornell.edu)

Abstract. Stratospheric aerosol injection (SAI) comes with a wide range of possible design choices, such as the location and timing of the injection. Different injection strategies can yield different climate responses; therefore, making informed future decisions on SAI requires an understanding of the range of possible climate outcomes. Yet to date, there has been no systematic exploration of a comprehensive set of SAI strategies. This limits the ability to determine which effects are robust across different strategies and which depend on specific injection choices, or to determine if there are underlying trade-offs between different climate goals.

This study systematically explores how the choice of SAI strategy affects climate responses. Here, we introduce four hemispherically-symmetric injection strategies, all of which are designed to maintain the same global mean surface temperature: an annual injection at the equator (EQ), an annual injection of equal amounts of SO_2 at 15° N and 15° S (15N+15S), an annual injection of equal amounts of SO_2 at 30° N and 30° S (30N+30S), and a polar injection strategy that injects equal amounts of SO_2 at 60° N and 60° S only during spring in each hemisphere (60N+60S). We compare these four hemispherically-symmetric SAI strategies with a more complex injection strategy that injects different quantities of SO_2 at 30° N, 15° N, 15° S, and 30° S in order to maintain not only the global mean surface temperature but also its large scale horizontal gradients. We find that the choice of SAI strategy notably affects the spatial distribution of aerosol optical depths, injection efficiency, and various surface climate responses. Among other findings, we show that injecting in subtropics produces more global cooling per unit injection, with the EQ and the 60N+60S cases requiring, respectively, 59 % and 50 % more injection than the 30N+30S case to meet the same global mean temperature target. Injecting at higher latitudes results in larger equator-to-pole temperature gradients. While all five strategies restore September Arctic sea ice, the high-latitude injection one is more effective due to the SAI-induced cooling occurring preferentially at higher latitudes.

https://doi.org/10.5194/egusphere-2023-117
Preprint. Discussion started: 2 March 2023

1 Introduction

Current climate projections suggest that under most emission scenarios the 1.5° C threshold of global mean temperature increase above pre-industrial levels set by the Paris Agreement is likely to be exceeded by 2040 or earlier (IPCC, 2021; Tebaldi et al., 2021; Dvorak et al., 2022). Meinshausen et al. (2022) showed that implementing all conditional and unconditional Paris Agreement pledges on time may limit global warming to just below 2° C. With the uncertainties in the implementation of carbon emission reductions, estimates of climate sensitivity, and severity of impacts of climate change, only relying on carbon emission reduction is likely insufficient to reduce the possibility of severe adverse climate impacts in the foreseeable future (Rogelj et al., 2016; Bamber et al., 2019; Anderson et al., 2020; Sherwood et al., 2020; Bjordal et al., 2020; MacMartin et al., 2022). This leads to the suggestion that stratospheric aerosol injection (SAI) could be an option at some point to reduce severe adverse impacts on climate and society. Such an approach would consist of injecting aerosols, or their precursors, in the lower stratosphere to reflect a small fraction of the incoming solar radiation back to space, as a result, lowering the global mean temperature.

To inform future decisions on SAI deployment, it is important to have a sufficient understanding of the range of possible climate responses under SAI; these would depend on both the scenario and strategy. Most existing SAI studies consider only a single scenario (i.e. a particular choice of background emission scenario, deployment start date and desired temperature target to be achieved with SAI) and only look at a single SAI strategy (i.e. a particular choice of injection latitude(s) and season(s)) (Kravitz et al., 2019; Visioni et al., 2020b; Tilmes et al., 2018; Irvine et al., 2019). MacMartin et al. (2022) described a set of specific scenario choices that cover a range of plausible futures, but all with a single strategy. Here we consider and compare a set of different SAI strategies under the same scenario. Collectively, these two studies capture two key dimensions of the range of possible climate responses to SAI.

Different SAI strategies can result in the same level of global cooling, but affect the regional surface climate differently (Visioni et al., 2020b; Kravitz et al., 2019; Lee et al., 2020, 2021; Zhang et al., 2022). Injecting SO_2 at the equator overcools the tropical region and undercools the high-latitude regions (Kravitz et al., 2019); injecting at 60° N primarily cools the northern hemisphere (Lee et al., 2023). Injecting SO_2 in the same latitude but in different seasons may also result in slightly different regional climate responses (Visioni et al., 2020b). Knowing the dependence of various climate responses on the choice of SAI strategies is crucial for comparing the benefits and risks of different SAI strategies. In addition, SAI will not bring the climate back to the same state as lowering the CO_2 concentration; instead, it will create a novel climate (Bala et al., 2010; Niemeier and Timmreck, 2015; Kravitz et al., 2017; Tilmes et al., 2018; Irvine et al., 2019). Knowing the range of possible climates and how close we can bring the climate to a reference state by SAI enables us to evaluate the limits of SAI and the trade-offs between achieving different climate objectives.

While different SAI strategies do not result in the same surface climate, the differences in surface climate responses between some SAI strategies are much easier to detect than between others. Zhang et al. (2022) estimated based on Community Earth System Model (CESM1) simulations that for a SAI-induced global cooling of 1–1.5° C, there are only 6–8 injection choices that produce detectably different surface climate responses. In that study, the surface climate responses from two injection choices are considered detectably different if the difference in temperature or precipitation responses are detectable at a 95 % confidence level over a 20-year period on more than 5 % of the Earth's area. The outcomes of other strategies can thus be estimated by a linear combination of these 6–8 injection choices, assuming linearity (MacMartin et al., 2017, 2019; Zhang et al., 2022).

Here, we introduce four hemispherically-symmetric injection strategies. These four new strategies along with the three existing strategies described in MacMartin et al. (2022), Lee et al. (2023), and Bednarz et al. (2022b) – i.e. a multi-objective strategy, an Arctic-focused strategy and a single-latitude injection case, respectively – collectively span the space of possible surface air temperature and precipitation responses for a global cooling of 1–1.5° C. Section 2 describes the climate model. Section 3 explains how this set of strategies are chosen and describes the simulation setup. Section 4 describes the simulation results of the four new strategies and compares them to the multi-objective strategy. The understanding that comes from the analysis of the differences between these strategies lays the foundation for future work on assessing the trade-offs between different SAI strategies and identifying better strategies.

2 Climate Model

All SAI strategies are simulated using version 2 of the Community Earth System Model with the middle atmosphere version of the Whole Atmosphere Community Climate model, version 6, as the atmospheric component, CESM2(WACCM6-MA) (Danabasoglu et al., 2020; Gettelman et al., 2019; Davis et al., 2022). CESM2(WACCM6-MA) is a fully coupled Earth system model which includes atmosphere, ocean, land, and sea ice components. The middle atmosphere (MA) version of WACCM6 uses chemistry mechanisms relevant for the stratosphere and mesosphere with a reduced set of tropospheric reactions (Davis et al., 2022), similar to the chemistry configuration in CESM1(WACCM). The horizontal resolution of CESM2(WACCM6-MA) is 0.95° in latitude and 1.25° in longitude, with 70 vertical layers extending from the Earth's surface to about 140 km in altitude, the same as in CESM1(WACCM) (Mills et al., 2017).

3 Simulations

Zhang et al. (2022) have shown that for a cooling level of 1–1.5° C, there are of order 6–8 distinct injection choices that yield detectably different surface climates. Although the estimate of 6–8 distinct injection choices was made using CESM1(WACCM) simulations, the conclusion is expected to be reasonably robust and model independent, as it depends principally on the constraints on the spatiotemporal distribution of aerosol optical depth (AOD) imposed by stratospheric circulation. Based on the conclusion in Zhang et al. (2022), here we choose a pragmatic set of seven potential latitudes of injection that could be combined in different ways: 60° N, 30° N, 15° N, the equator, 15° S, 30° S and 60° S. Injections at high latitudes (i.e., 60° N and 60° S) are conducted at a constant rate only in spring (as in Lee et al. (2021)), and injections at other latitudes are conducted at a constant rate throughout the year. The AOD design space spanned by this pragmatic set of injection choices includes all AOD patterns that in CESM yield detectably different surface climate responses for a global cooling level of 1–1.5° C, as described

https://doi.org/10.5194/egusphere-2023-117
Preprint. Discussion started: 2 March 2023

in Zhang et al. (2022). In the following paragraphs, we introduce a possible set of seven injection strategies and explain our choice. We note that one could pick a different set of seven injection strategies based on these seven injection choices, which would also be linearly independent and span the same AOD design space.

A multi-objective strategy, using annually-constant SO_2 injection at 30° N, 15° N, 15° S, and 30° S, was developed by Kravitz et al. (2017) and has been repeated in Tilmes et al. (2018, 2020), MacMartin et al. (2022) and Richter et al. (2022). This strategy adjusts the SO_2 injection rates across the four latitudes to maintain the global mean surface temperature (T0), the interhemispheric temperature gradient (T1) and equator-to-pole temperature gradient (T2). Global mean surface temperature is the metric used by the United Nations Framework Convention on Climate Change (UNFCCC) to operationalize climate change goals in the Paris Agreement (UNFCCC, 2015), thus a reasonable metric to consider as a target for SAI (MacMartin et al., 2022). However, while managing the interhemispheric temperature gradient is motivated by the desire to reduce shifts in tropical precipitation, the specific injection rates have been shown to vary even in different versions of the same Earth System Model (Fasullo and Richter, 2023).

Given the uncertainty and model dependence of the hemispheric asymmetry in injection rates needed to maintain T1, we consider four hemispherically-symmetric strategies that maintain only T0: injecting solely at the equator (EQ), injecting the same amount at 15° N and 15° S (15N+15S), injecting the same amount at 30° N and 30° S (30N+30S), and injecting the same amount at 60° N and 60° S in springtime only in each hemisphere (60N+60S) (Table 1). While we do not expect these to fully balance the interhemispheric temperature gradient T1 in CESM2(WACCM6), these represent plausible strategies that are not dependent on the model-dependent T1 response; these are also all simpler than the multi-objective strategy and thus would be more straightforward to replicate in other climate models.

In addition to the multi-objective strategy and the four hemispherically-symmetric strategies, a complete set of strategies spanning the space of the seven injection choices described by Zhang et al. (2022) would also include two other strategies, such as a spring injection at 60° N described by Lee et al. (2023) and an annually-constant injection at 30° N described by Bednarz et al. (2022b). However, we note that injecting solely at either 60° N or 30° N will primarily cool the northern hemisphere, which would result in a significant perturbation of the interhemispheric temperature gradient and the associated location of tropical precipitation. Thus, these two single-latitude injections are already known to not be an appropriate strategy for targeting global mean temperature and as such are not included in the analysis discussed here.

All of the strategies considered herein are simulated under the same scenario (i.e., the same background greenhouse gas emissions, start date for SAI deployment, and global mean temperature target). The background emission scenario used here is the Shared Socioeconomic Pathway (SSP) 2-4.5 (Meinshausen et al., 2020), a ‘middle-of-the-road’ pathway in which the world is facing medium challenges to mitigation and adaptation (IPCC AR6). This background emission scenario is roughly consistent with the Paris Agreement’s Nationally Determined Contributions (Burgess et al., 2021; UNEP, 2021-10). All of these injection strategies are simulated from the beginning of 2035 to the end of 2069. The average over 2020–2039 in the model is chosen to be representative of when future climate might reach 1.5° C above pre-industrial levels (MacMartin et al., 2022). Here, to increase the ability to distinguish between effects of different strategies, we choose an additional 0.5° C cooling relative to the 1.5° C target from the Paris Agreement. This new temperature target of 1.0° C above pre-industrial levels corresponds

Table 1. SAI Strategies evaluated in this study. All simulations start in January 2035 and end in December 2069.

Strategy	Injection rate and latitude(s)	Injection season	Injection altitude (km)	Design objective(s)
60N+60S	equal at 60° N and 60° S	Spring (MAM at 60° N, SON at 60° S)	15.0	T0
30N+30S	equal at 30° N and 30° S	Annually constant	21.5	T0
15N+15S	equal at 15° N and 15° S	Annually constant	21.5	T0
EQ	equator	Annually constant	21.5	T0
Multi-Objective (MacMartin et al., 2022)	variable at 30° N, 15° N, 15° S, and 30° S	Annually constant	21.5	T0/T1/T2

to the average global mean temperature over 2008–2027 in CESM2(WACCM6), which we will use as the reference period for comparison. All simulations herein aim to ultimately cool the planet to this 1.0° C target, but as the model temperature in 2035 (i.e. at the start of SAI deployment) is already roughly at 1.5° C above pre-industrial levels, the cooling target gradually ramps down to the desired 1.0° C target over the first 10 years of simulation and then stays the same for the following years. This corresponds to the SSP2-4.5:1.0 scenario in MacMartin et al. (2022).

Injection rates are determined by a controller, which has a feedforward component and a feedback component. The injection rate in each year is first calculated by the feedforward based on our estimate of the sensitivity to injection (based on 10-year simulations in (Visioni et al., 2022), and then corrected by a Proportional Integral (PI) controller (MacMartin et al., 2014; Kravitz et al., 2017). At the start of each model year, the controller takes the output values from the previous year and calculates the injection rate for the forthcoming year. All of the SAI and SSP2-4.5 simulations consist of three ensemble members each.

4 Results

Here we present the injection rates, stratospheric AOD values, as well as global and regional surface climate responses under the four hemispherically-symmetric SAI strategies and the multi-objective strategy. All of these five injection strategies are designed to maintain the same global mean surface temperature. We assume that all timeseries analyzed here follow a first-order autoregressive (AR(1)) process, and calculate the standard errors with the effective sample size estimated by the lag-1 autocorrelation (Wilks, 2019).

4.1 Large-scale global climate responses

Figure 1(a) shows the time evolution of the global mean surface temperature in all simulations. In the last 20 years of injection, T0 in all SAI strategies considered here is maintained within one standard deviation (σ_{T_0}=0.24° C) from the target value; this requires around 1.4° C global cooling compared to the SSP2-4.5 case without SAI. As discussed in Section 2, the multi-objective strategy is the only SAI strategy discussed here that is also designed to maintain the interhemispheric temperature gradient (T1) and the equator-to-pole temperature gradient (T2) in addition to T0. T1 and T2 are defined as the linear and quadratic meridional dependence of the zonal-mean temperature (Kravitz et al., 2016):

$$T_1 = \frac{1}{A} \int_{-\pi/2}^{\pi/2} T(\psi) sin(\psi)\, \mathrm{d}A \tag{1}$$

$$T_2 = \frac{1}{A} \int_{-\pi/2}^{\pi/2} T(\psi) \frac{1}{2}(3 sin^2(\psi) - 1)\, \mathrm{d}A \tag{2}$$

where ψ is the latitude in radians, $T(\psi)$ is the zonal-mean temperature at latitude ψ and A is the surface area of the Earth. A positive value of T1 means that the northern hemisphere (NH) is warmer than the southern hemisphere (SH). A negative value of T2 means that polar regions are colder than the tropics; an increase in the temperature difference between the equator and poles will decrease T2.

Without SAI, T1 increases over time under climate change because of differences in the land cover between the hemispheres (Fig. 1(b)). We find that all SAI strategies considered here overcompensate T1, which corresponds to a reduction in temperature gradient between the NH and SH compared to the reference period. The overcompensation of T1 is likely linked to the reduction in cloud cover in the SH subtropics due to the strong cloud response to elevated CO_2 levels in the SH in CESM2(WACCM6) (Fasullo and Richter, 2023). As a result, greater radiative heating needs to be mitigated in the SH. The same SAI strategies do not overcompensate T1 in other models. For example, in CESM1(WACCM), the equatorial injection which yields greater AOD in the NH roughly maintained T1, as described in (Kravitz et al., 2019). With greater radiative heating needed to be mitigated in the SH in CESM2(WACCM6) compared to CESM1(WACCM), the equatorial injection ends up overcompensating T1 in this model.

Being designed to explicitly impact the interhemispheric temperature gradient, the multi-objective strategy better maintains T1 at the reference period value compared to the SAI strategies that are designed to only maintain T0. We note that there is still a slight overcompensation of T1 in the multi-objective strategy. It is possible that the control gains in the controller are not large enough such that T1 in the multi-objective strategy has not yet converged to the targeted value.

Figure 1(c) shows the evolution of the equator-to-pole temperature gradient. T2 increases over time under SSP2-4.5 as the result of the warming being much faster in the Arctic than in the mid- and low-latitudes. The magnitude of Arctic amplification has been estimated to be a factor between 1.5 and 4.5 (Holland and Bitz, 2003; Previdi et al., 2021). All SAI strategies considered here reduce T2 compared to the SSP2-4.5 simulation. The strategies injecting outside of the tropical pipe, i.e. 30N+30S and 60N+60S, overcompensate T2 compared to the reference period. This overcompensation occurs because injecting SO_2

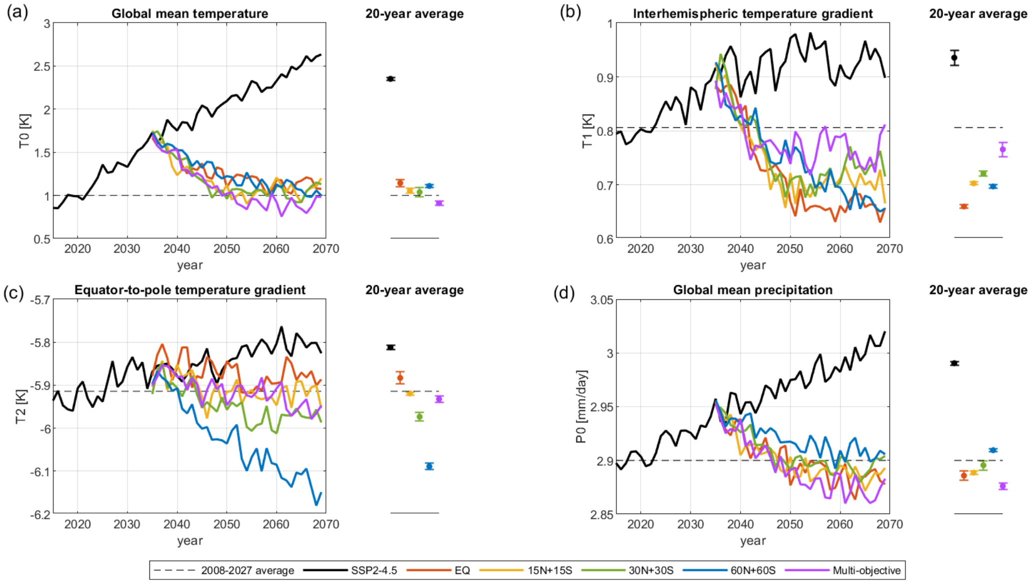

Figure 1. Time evolution of (a) global mean surface temperature relative to the pre-industrial level (T0), (b) interhemispheric temperature gradient (T1), (c) equator-to-pole temperature gradient (T2), and (d) global mean precipitation (P0). Each solid line represents the ensemble mean of each injection strategy. The dashed line represents the 20-year average during the reference period (2008–2027). The dots on the right of each panel represent the 20-year average over 2050–2069; the uncertainties in the calculated 20-year averages are estimated by ±1 standard error, and represented by the error bars.

outside of the tropics results in more cooling at mid- and higher latitudes, thus offsetting Arctic amplification and leading to more reduction in T2.

Figure 1(d) shows the evolution of global mean precipitation. With increasing GHG forcing, global mean precipitation increases over time in the SSP2-4.5 simulation. This response has been observed under rising GHG levels across climate models (IPCC, 2021), and arises because global mean precipitation is governed by the availability of energy (Allen and Ingram, 2002; O'Gorman et al., 2012). With the added SAI forcing, the global mean precipitation is reduced, consistent with the associated decrease in global mean temperature, and is overcompensated relative to the global mean precipitation in the reference period (P0=2.9 $\mathrm{mm\ day^{-1}}$), except for the 60N+60S case. This overcompensation in precipitation relative to the associated decrease in temperature was observed in many previous studies using either solar reduction (Bala et al., 2008; Tilmes et al., 2013) or stratospheric aerosols (Niemeier et al., 2013; Lee et al., 2020). We find that injections at lower latitudes yield a stronger overcompensation in precipitation, as shown in Fig. A1. This is likely because tropical cooling has a comparatively larger impact on global mean precipitation compared to the surface cooling that occurs outside the tropics, so the strategies with stronger tropical cooling yield stronger overcompensation in precipitation (Fig. A1). In addition, the increase in tropospheric static stability as the result of aerosol-induced lower stratospheric heating can also contribute to the reduction of global mean precipitation (Simpson et al., 2019). More detailed discussions are provided in the appendix.

https://doi.org/10.5194/egusphere-2023-117
Preprint. Discussion started: 2 March 2023

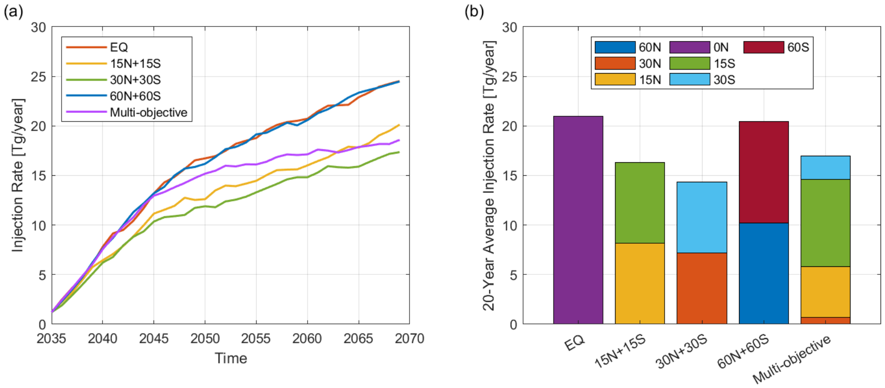

Figure 2. (a) Total amount of SO_2 injected into the stratosphere per year [Tg yr^{-1}], and (b) annual injection of SO_2 [Tg yr^{-1}] at each latitude averaged over the last 20 years (2050–2069), for each SAI strategy. The 20-year average injection rates of EQ, 15N+15S, 30N+30S, 60N+60S, and multi-objective strategies are 21, 16, 14, 20, and 17 Tg yr^{-1}, respectively. Injection rate of each strategy is averaged over three ensemble members.

4.2 Injection rates and AOD

Figure 2(a) shows the evolution of the total SO_2 injection rate in each SAI strategy, and Fig. 2(b) the 20-year (2050–2069) average injection rates. Even though all five injection strategies aim to maintain the global mean surface temperatures at the same levels, different amounts of SO_2 injections are required in each case to achieve this. Among the five strategies, the 30N+30S strategy requires the least amount of injection, and the EQ and 60N+60S strategies require the largest amount of injection, which are, respectively, 59% and 50% more than the injection required by the 30N+30S strategy. The multi-objective strategy injects the majority of SO_2 in the Southern Hemisphere (Fig. 2(b)); the average injection rate during 2050–2069 at 30° S, 15° S, 15° N, and 30° N is 2.4, 8.8, 5.1, and 0.7 Tg yr^{-1}, respectively. This hemispheric asymmetry in the distribution of SO_2 injections is likely due to the rapid cloud responses to elevated CO_2 levels in CESM2(WACCM6), resulting in greater radiative heating that needs to be mitigated in the SH (Fasullo and Richter, 2023).

The efficiency of AOD and of global mean surface cooling per unit injection for these five strategies is shown in Fig. 3(a) and (c), respectively. These results indicate that it is more efficient to inject SO_2 in mid-latitudes than in the tropics or high latitudes. The low efficiency in the equatorial injection is partially due to larger aerosol particles being formed near the tropics as the aerosols are relatively confined inside the tropical pipe and, hence, more prone to coagulation and condensation (Fig. 4(b); see also (Visioni et al., 2017; Kravitz et al., 2019). The relatively larger aerosol effective radius in the equatorial injection case reduces the AOD per unit mass of sulfate, and also the aerosol lifetime in the stratosphere due to increased sedimentation. In addition, the warming of the cold point tropopause as the aerosols absorb some of the solar and terrestrial radiation is largest for the equatorial injection strategy. This results in the strongest increase in stratospheric water vapor which, as a greenhouse gas, offsets some of the direct aerosol cooling (Visioni et al., 2021; Bednarz et al., 2022a); this effect thus requires increased SO_2 injection rates to compensate.

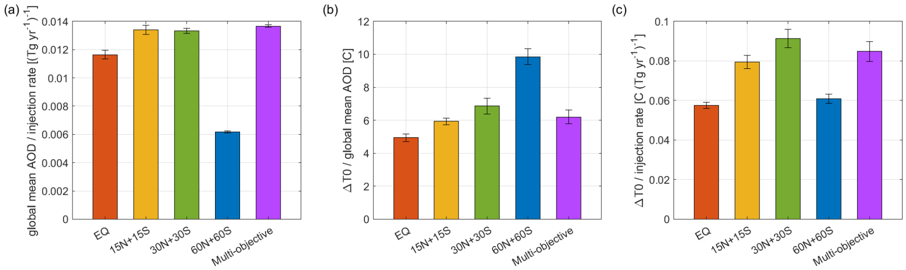

Figure 3. (a) Global mean AOD per unit of injection rate [$(\mathrm{Tg\,yr^{-1}})^{-1}$], (b) global cooling per unit of global mean AOD [C], and (c) global cooling per unit of injection rate [$\mathrm{C}(\mathrm{Tg\,yr^{-1}})^{-1}$], calculated over the 20-year period of 2050–2069. Error bars represent the standard error of the mean.

The notably lower efficiency of AOD per unit of injection in the 60N+60S strategy is because aerosols injected at high latitudes have a much shorter lifetime due to the proximity to the downward part of the stratospheric Brewer-Dobson circulation and stratosphere-troposphere exchange areas, thus faster transport to the troposphere where they are removed. The average lifetime of the injected stratospheric aerosol (calculated as the ratio of stratospheric SO_2 burden to injection rate) is 1.36±0.009 years, 1.39±0.011 years, 1.26±0.010 years and 0.58±0.004 year for EQ, 15N+15S, 30N+30S, and 60N+60S respectively. Although 60N+60S has the lowest efficiency of AOD per unit injection, it yields the highest efficiency of global cooling per unit of global mean AOD (Fig. 3(b), 4(b)), due to its strong effectiveness in offsetting Arctic amplification (Zhao et al. (2021); see also Section 4.1), as the initial cooling from high latitude AOD is amplified by the high latitude feedbacks (Holland and Bitz, 2003; Serreze and Barry, 2011; Hahn et al., 2021; Previdi et al., 2021). Figure 3(b) also indicates that the efficiency of global cooling per unit AOD increases with latitude.

Nonlinearity is observed in the efficiency of AOD per unit injection, more notable in the low- and mid-latitude injections (Fig. 4(a)). Higher concentration of SO_2 in the stratosphere results in larger aerosol particles which in turn sediment out faster, thus leading to smaller AOD per unit mass of sulfate (Niemeier and Timmreck, 2015; Kleinschmitt et al., 2018; Visioni et al., 2020a). Compared to high-latitude injection, low- and mid-latitude injections result in larger aerosol effective radius (Fig. 4(b)).

Figure 5 shows the latitudinal distributions of the zonal mean AOD and zonal mean temperature changes for different SAI strategies, averaged over the last 20 years of the simulations (2050–2069). Injecting in the tropics yields an asymmetrical AOD distribution between hemispheres, with higher AOD in the NH and lower AOD in the SH. This asymmetry arises as the northern hemisphere has a stronger Brewer-Dobson circulation than the southern hemisphere (Butchart, 2014). In contrast, injecting in the extratropics results in a relatively hemispherically-symmetric distribution of AOD. With the multi-objective strategy, AOD in the SH is notably higher than the NH, consistent with the largest injection rates at 15° S (Richter et al., 2022) that are required to minimize changes in the interhemispheric surface temperature gradient (Fig. 5(b)). Although the hemispherically-symmetric strategies yield similar levels of AOD at high latitudes in both hemispheres, the cooling in the Arctic is much larger than the Antarctic due to the Arctic amplification effect discussed above (Fig. 5(b-c)). Figure 6 shows the spatiotemporal distribution

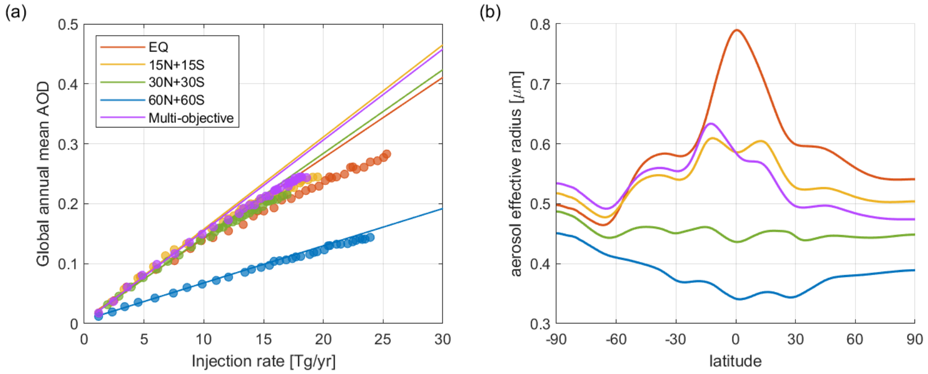

Figure 4. (a) The relationship between Injection rate and corresponding global mean AOD in each year of each simulation, and (b) latitudinal distribution of concentration-weighted aerosol effective radius in the stratosphere, averaged over the last 20 years (2050–2069). The lines in (a) are linear fits under low injection rates (i.e. when the injection rate is lower than 10 Tg yr^{-1}).

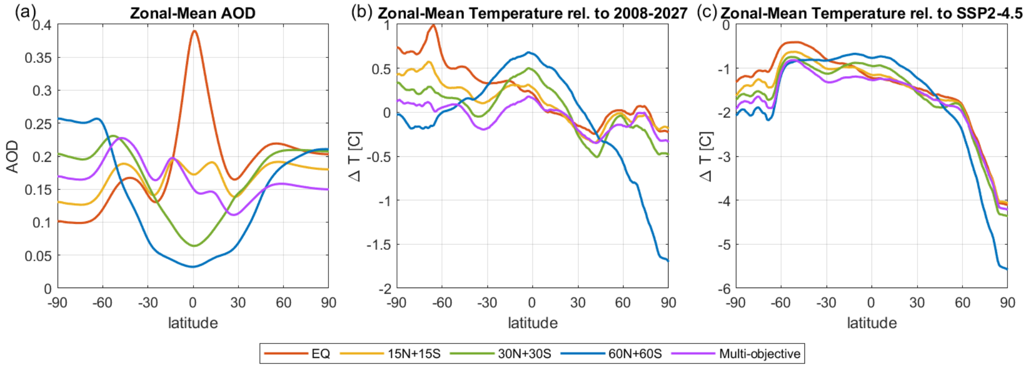

Figure 5. Latitudinal distribution of (a) zonal-mean AOD per degree Celsius of global cooling, (b) zonal-mean surface air temperature response relative to the 20-year average of the reference period, 2008–2027, and (c) zonal-mean surface air temperature response relative to the same 20-year period (2050–2069) under the SSP2-4.5 scenario.

of stratospheric AOD for all five SAI strategies. We normalize the values of AOD by the associated amount of global mean cooling under each SAI strategy. The simulated distribution of AOD depends on the latitudinal transport of air toward the poles, which is affected by both the Brewer-Dobson circulation and the strength of the stratospheric polar vortex (Visioni et al., 2020a). Due to seasonality in the strength of the stratospheric transport, AOD for annual injections also exhibits a marked seasonal cycle, with extratropical AOD maximizing in general in winter and spring at each hemisphere. In the case of the high-latitude seasonal injections, AOD maximizes in the mid- and high- latitudes in the season following the season of SO_2 injections because it takes about 1 month for injected SO_2 to oxidize into aerosols (Lee et al., 2021).

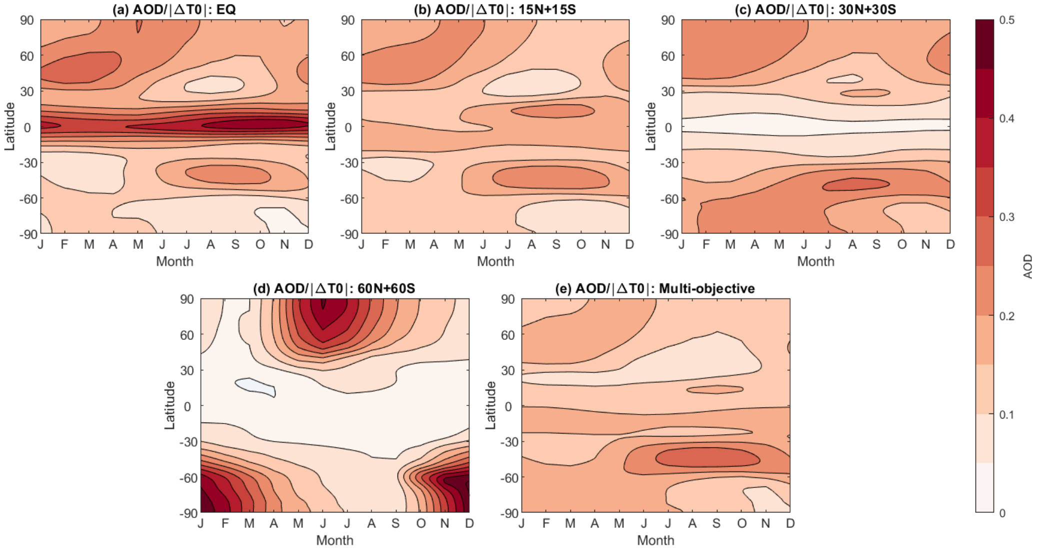

Figure 6. Simulated seasonal cycle of AOD at each latitude for 1° C of global mean cooling under each SAI injection strategy.

4.3 Regional surface climate responses

Sections 4.1-4.2 above focused on the large-scale responses to different SAI strategies; we now evaluate the corresponding changes in regional surface climate. We average the annual mean surface air temperatures and precipitation minus evaporation (P-E) over the 2050–2069 period and all three ensemble members, and calculate the changes relative to the reference period (2008–2027). The associated precipitation responses are shown in Fig. A2 and described in more detail in the appendix. Welch's t-test is performed to evaluate whether these regional changes are statistically significant. Since this test assumes that sampled data are independent, we perform the t-tests using the estimated effective sample size by assuming temperatures, precipitations, and P-E all follow a first-order autoregressive (AR(1)) process (Wilks, 2019).

4.3.1 Surface air temperature

Figure 7 shows the simulated changes in surface air temperatures. In SSP2-4.5, most areas on the Earth are warmer than the reference period, with the largest warming found in the Arctic region due to Arctic amplification. Overall, the temperature increase over land is higher than over the ocean (Fig. 7a). The exception to the overall warming trend is a region in the North Atlantic Ocean which shows a cooling pattern (so called 'North Atlantic warming hole') that is related to the weakening of Atlantic meridional overturning circulation (AMOC) (Tilmes et al. (2020), Fasullo and Richter (2023); see also Fig. 12). The North Atlantic warming hole has also shown up in simulations in other climate models (Chemke et al., 2020; Keil et al., 2020) as well as in the RCP8.5 scenario simulated in CESM1(WACCM) (Tilmes et al., 2017). In addition to the reduced northward heat transport due to the weakening of AMOC, the formation of the warming hole has been shown to be also driven by increased ocean heat transport from the warming hole to higher latitudes and a shortwave cloud feedback (Keil et al., 2020).

Figures 7(b)-(f) show that all SAI strategies effectively counteract the large-scale surface warming, as illustrated by the large fraction of surface area showing no statistically significant temperature difference relative to the reference climate. With SAI, the percentage of area with no statistically significant change ranges from 71 % to 84 %, while only 15 % of total area has no statistically significant difference without SAI. Despite similar magnitudes of global mean cooling (Fig. 1a), different SAI strategies yield different regional temperature responses. The EQ strategy undercools the Southern Hemisphere, which is due to greater radiative heating that needs to be mitigated in SH in CESM2(WACCM6) (Fasullo and Richter, 2023). In contrast, the 60N+60S strategy overcools the Arctic and undercools the tropics because the injections are focused at higher latitudes and the resulting aerosols are rapidly transported poleward and downward by the Brewer-Dobson circulation.

In all simulations (Fig. 7), the surface air temperature in a region in the North Atlantic Ocean is lower than the reference period, similar to the response found in the SSP2-4.5 simulation. This phenomenon is caused by the weakening of AMOC, which is discussed above and in more detail in Section 4.6. We also find consistent temperature changes over the Pacific Ocean across all SAI simulations, with relative warming in the eastern Pacific in both its equatorial and northern regions compared to the reference period. The pattern corresponds to the positive phase of the El-Nino Southern Oscillation (ENSO; e.g. McGregor et al., 2022). It is likely the result of the reduction in the strength of the equatorial Walker Circulation due to aerosol heating in the lower stratosphere (Simpson et al., 2019), as solar reduction doesn't significantly change the Walker Circulation (Guo et al., 2018).

To evaluate how well these strategies compensate for the change in regional temperature under climate change, we calculate an ensemble mean area-weighted root mean square (rms) temperature change comparing the 2050–2069 average to the reference period (2008–2027) (Fig. 8(a)). We also calculate the rms temperature change due to natural variability alone. This is done by first detrending the annual mean temperature over 2008–2027 at each gridbox in the three ensemble members, and then calculating the area-weighted rms standard error of the processed data assuming an AR(1) autocorrelation process. If an SAI strategy fully compensates the GHG-induced regional temperature changes, then on average the rms response will be similar to the rms change due to natural variability alone.

We find that in all SAI strategies, the rms temperature change is larger than the rms temperature change one would expect due to natural variability alone (i.e. 0.08° C, represented by the dashed line in Fig. 8a). Among the SAI strategies considered here, the multi-objective strategy best minimizes the regional temperature change, as indicated by the lowest rms temperature change (rms T=0.38° C). The 60N+60S strategy results in an uneven cooling with the highest rms temperature change (rms T=0.57° C), but still much smaller than the rms temperature change in SSP2-4.5 without SAI (rms T=1.53° C).

4.3.2 Precipitation minus evaporation

The net flux of water from the atmosphere to the Earth's surface is described by precipitation minus evaporation (P-E). Under the SSP2-4.5 scenario, only 33 % of the land area has a statistically significant change in P-E compared to the reference period (Fig. 9a). We find that none of the SAI strategies fully compensates for the regional hydrological changes caused by rising greenhouse gas levels (Fig. 9(b)-(f)). In particular, all SAI strategies give rise to mean rms P-E and precipitation responses that are larger than those from natural variability alone (which are estimated as approximately 0.06 $\mathrm{mm\ day^{-1}}$ and 0.09 mm

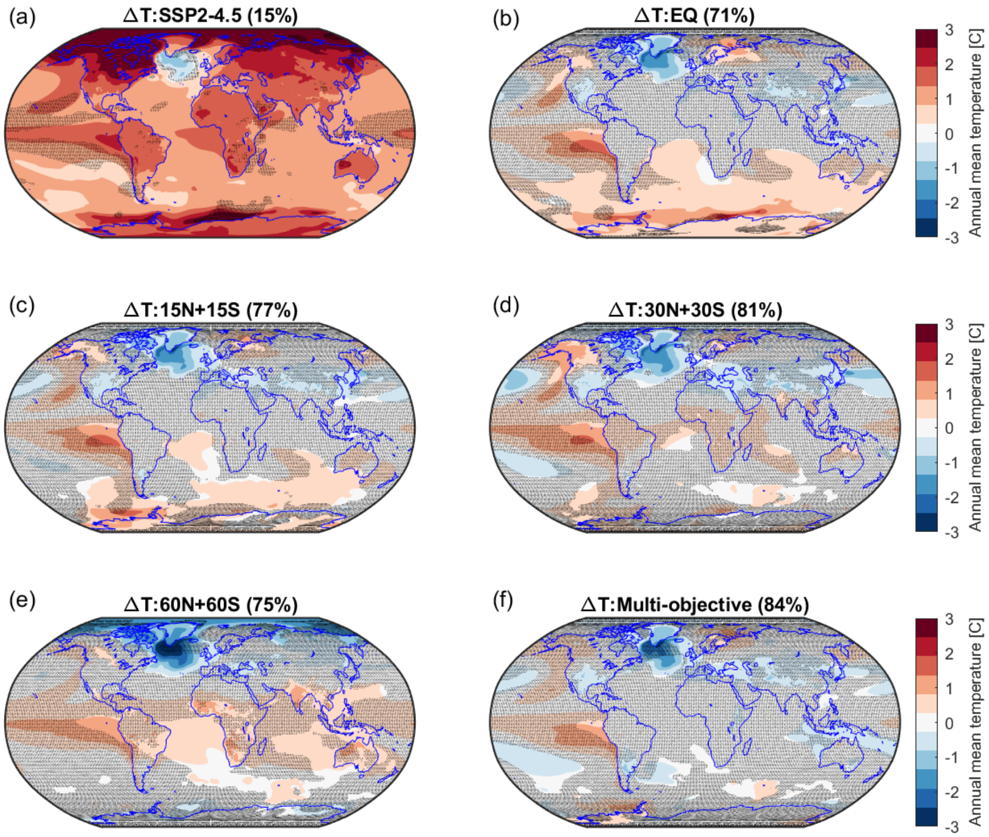

Figure 7. Changes in surface air temperature, averaged over 2050–2069, compared to the reference period (2008–2027) for (a) SSP2-4.5 and (b)-(f) different SAI injection strategies. Shaded areas indicate where the change relative to the reference period is not statistically significant based on a two-tailed Welch's t-test with a confidence level of 95 %. The percentage of area with no statistically significant change in surface air temperature is listed in the title of each map.

day^{-1} for P-E and precipitation changes, respectively (Fig. 8(b)-(c)). In addition, while the SAI scenarios have roughly the same percentage of the land area with statistically significant change in P-E (20–27 %), the regional changes in P-E vary between the different SAI strategies as well as the SSP2-4.5 run (Fig. 9). For example, the EQ strategy makes central Africa drier, while the P-E response in central Africa is not statistically significant under other SAI strategies. Also, the reduction in P-E over North India is statistically significant under 30N+30S and 60N+60S strategies, but not statistically significant under the other strategies.

The difference in rms P-E and precipitation responses between SAI simulations and the SSP 2-4.5 simulation is notably smaller than the difference in temperature responses. When compared against the same period of the SSP2-4.5 simulation, the

https://doi.org/10.5194/egusphere-2023-117
Preprint. Discussion started: 2 March 2023

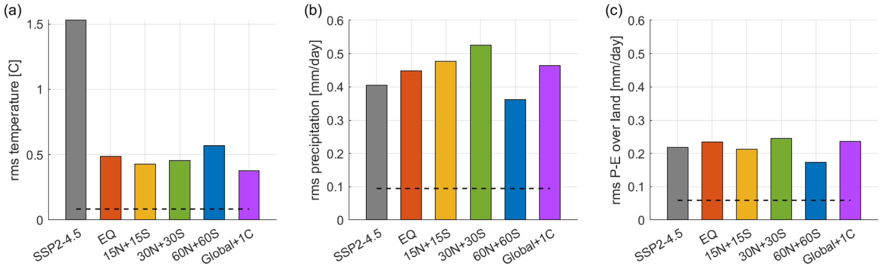

Figure 8. Area-weighted root mean square deviation between the (a) temperature, (b) precipitation, and (c) P-E over land averaged over 2050–2069 and the reference period (2008–2027). The dashed lines represent the area-weighted root mean square of each quantity due to natural variability alone.

.

difference in rms P-E response over land is no more than 12 % for any of the SAI strategies (Fig. 8(c)). For the corresponding changes in precipitation over the whole Earth surface (i.e. both land and ocean), the difference is no more than 30 % (Fig. 8(b)). More detailed analysis of the precipitation response is provided in the appendix.

4.4 Intertropical convergence zone

The Intertropical Convergence Zone (ITCZ) is a region of heavy precipitation near the equator, where the northeast and southeast trade winds collide (Byrne et al., 2018). Different metrics have been used in previous studies to define the ITCZ location, such those based on the precipitation centroid (e.g., Frierson and Hwang, 2012; Donohoe et al., 2013; Byrne et al., 2018; Lee et al., 2020) or based on atmospheric mass circulation (e.g., Hari et al., 2020; Cheng et al., 2022). Here, we define the ITCZ location as the latitude near the equator where the zonal mean meridional streamfunction at 500 hPa changes sign. The streamfunction at each latitude is calculated using the following equation:

$$\Psi = \frac{2\pi a cos(\phi)}{g} \int_{0}^{p} [v] \, \mathrm{d}p' \qquad (3)$$

where $[v]$ is the zonal mean meridional velocity, a is the Earth's radius, ϕ is latitude, and p is 500 hPa. The ITCZ location is approximated using linear interpolation of the centers of two consecutive grid cells that have meridional circulations of opposite directions.

Under GHG forcing alone, the latitude of ITCZ shifts southward from its location in the reference period (Fig. 10(a)). All hemispherically-symmetric SAI injection strategies shift the latitude of ITCZ further south, consistent with the stronger associated cooling in the NH than in the SH (Fig. 5(b)-(c)). The multi-objective strategy, on the other hand, shifts the latitude of ITCZ northward from that due to GHGs alone, but still south of the ITCZ position in the reference period.

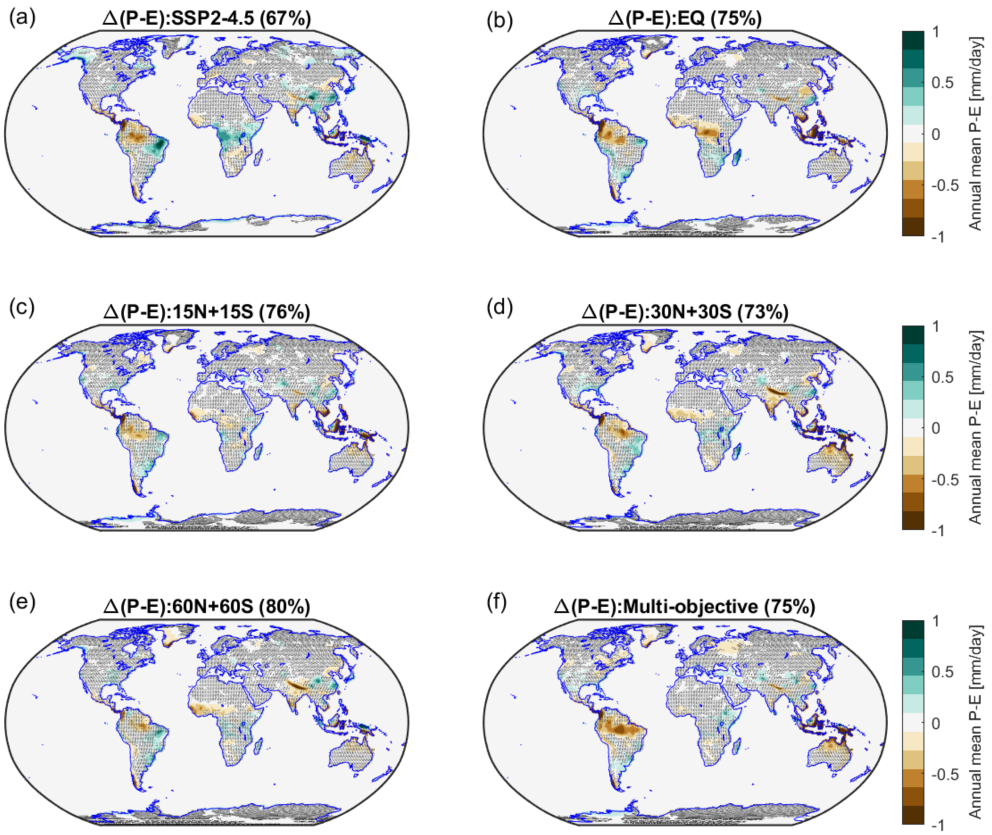

Figure 9. Changes in precipitation minus evaporation (P-E) over land averaged over 2050–2069, compared to the reference period (2008–2027) for (a) SSP2-4.5 and (b)-(f) different SAI injection strategies. Shaded areas indicate where the response is not statistically significant based on a two-tailed Welch's t-test with a confidence level of 95 %. The percentage of land area with no statistically significant change in P-E is listed in the title of each map.

4.5 Arctic sea ice

The Arctic sea ice extent is expected to decrease in response to increasing global warming. If the current emissions of 40 Gt yr^{-1} CO_2 continues without reduction, the Arctic Ocean is very likely to become ice free during summer before mid-century (Notz and Stroeve, 2018). The effectiveness of restoring Arctic sea ice through stratospheric aerosol injection is evaluated through comparing the predicted September Arctic sea ice extent (SSI) under SAI strategies and the SSP2-4.5 scenario. Figure 11(a) shows that all these five SAI strategies increase SSI to at least the reference period level by the year 2070. After around the year 2050, SSI starts to stabilize around the reference period level in the low- and mid-latitude injection cases, while SSI continues increasing in the high latitude injection case; the latter is consistent with the associated surface temperature

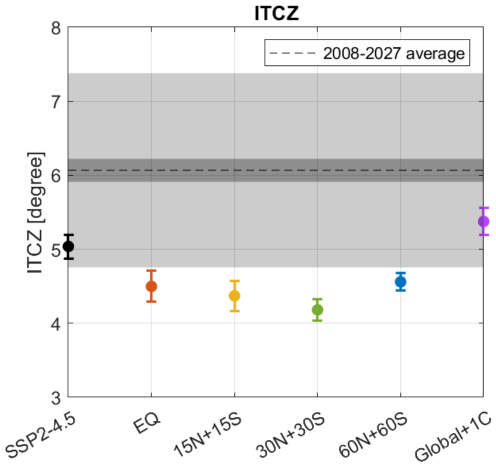

Figure 10. The 20-year (2050–2069) average (dots) and standard error (vertical bars) of the mean latitude of ITCZ for SSP2-4.5 and the different SAI strategies. The dashed horizontal line represents the mean latitude of ITCZ during the reference period (2008–2027) and the shaded areas represent the corresponding standard error (dark gray) and standard deviation (light gray).

.

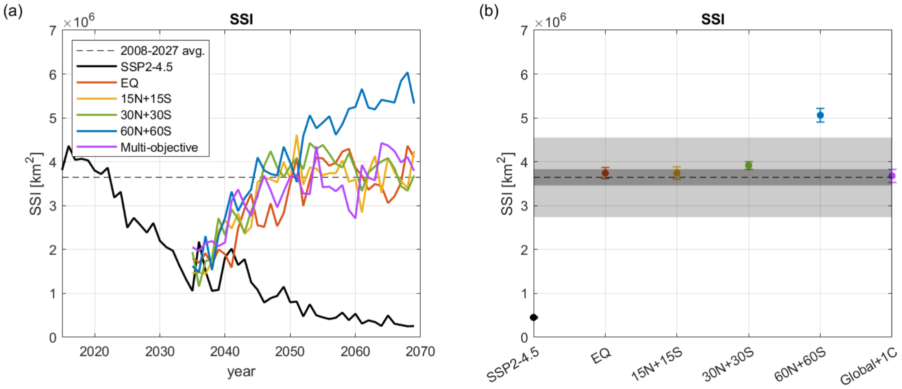

Figure 11. (a) Time evolution of September Arctic sea ice extent (SSI) for SSP2-4.5 and the different SAI strategies. (b) The 20-year (2050–2069) average (dots) and standard error (vertical bars) of SSI for SSP2-4.5 and the different SAI strategies. The dashed horizontal line represents the average SSI during the reference period (2008–2027) and the shaded areas represent the corresponding standard error (dark gray) and standard deviation (light gray).

.

changes (Fig. 7) and their equator-to-pole gradients (Fig. 1(c)). The 60N+60S strategy increases SSI by the highest amount; the 20-year (2050–2069) average of SSI is about 5×10^6 km^2, which is 1.4×10^6 km^2 more than the reference period level. The overcompensation of SSI in the 60N+60S strategy is mainly because of the largest fraction of aerosols found in the polar region.

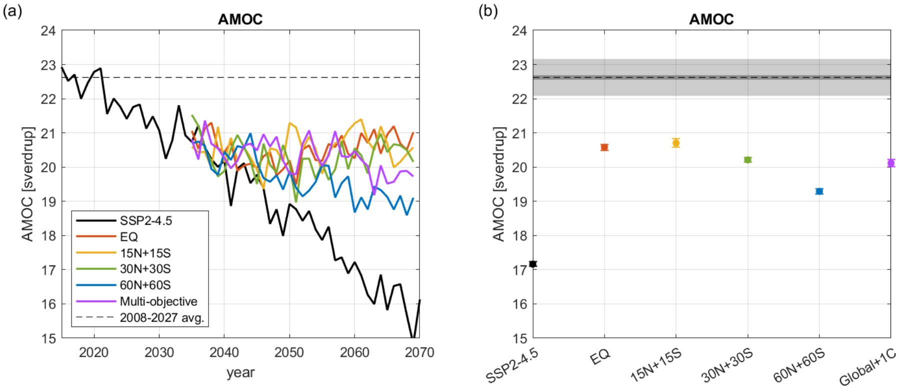

Figure 12. (a) Time evolution of the strength of the Atlantic Meridional Overturning Circulation (AMOC) under different SAI injection strategies over the period of 2035-2069, calculated as the maximum over depth and latitude of the meridional streamfunction in the North Atlantic. (b) As in Fig. 11(b) but for the strength of the AMOC.

.

4.6 Atlantic meridional overturning circulation

Section 4.3 and Fig. 7 show that all simulations yield a region in the North Atlantic Ocean that is cooler than the reference period. In accord, Fig. 11(a) shows that in CESM2(WACCM6), AMOC continues to weaken over the 21st century under SSP2-4.5, which is consistent with the predictions from other climate models (Chemke et al., 2020; Keil et al., 2020; IPCC, 2021). AMOC moves warm water northward at the surface from the tropics and cold water southward at the bottom of the ocean from the North Atlantic (Rahmstorf, 2002). As AMOC weakens, less heat is transported northward to the North Atlantic, which causes the decrease in the surface air temperature over that region (Danabasoglu, 2008).

We find that low- and mid-latitude injections are better at recovering AMOC than the high-latitude injections. Whilst the low- and mid-latitude injections do not restore AMOC back to the reference period, they do prevent further weakening of AMOC and keep AMOC at a strength similar to that in the year 2035 when injections are started. In comparison, AMOC continues weakening under the high-latitude SAI strategy, but at a much lower rate compared to the SSP2-4.5 case. The weakening of AMOC relative to the reference period is likely the main cause of the consistent cooling pattern over the North Atlantic in every strategy in Fig. 7.

We find a slight positive trend in the AMOC strength for both the equatorial and 15N+15S strategies, and a negative trend in the Multi-objective and 60N+60S ones. It could be possible that the AMOC strength may eventually be restored to the reference period level with the low-latitude injections in this particular climate model; however, since the variability of AMOC is at multidecadal timescales, our simulations would need to be extended for a number of decades in order to determine this, which is beyond the scope of the current study.

https://doi.org/10.5194/egusphere-2023-117
Preprint. Discussion started: 2 March 2023

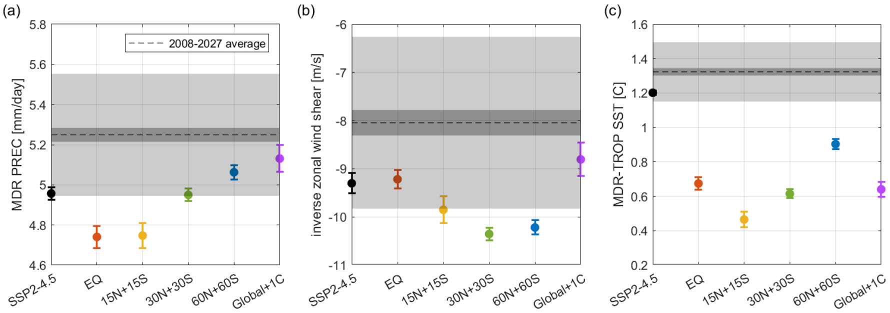

Figure 13. As in Fig. 10 but for the tropical cyclone frequency metrics: (a) the average precipitation in the main development region (MDR, see text for details), (b) inverse vertical zonal-wind shear in MDR, and (c) relative sea surface temperature difference between MDR and the tropics.

4.7 Tropical cyclone frequency

Existing studies show that climate change will decrease the overall tropical cyclone (TC) frequency but increase the frequency of the most intense ones (Bengtsson et al., 2007; Knutson et al., 2010; Camargo, 2013). Figure 13 evaluates the North Atlantic TC activity based on three TC indices that are described in Dunstone et al. (2013) and Jones et al. (2017). These TC indices evaluate the average precipitation in the main development region (MDR, defined as 5-20° N and 15-85° W), the inverse vertical zonal-wind shear between 850 and 250 hPa in the MDR, and the sea surface temperature (SST) difference between the MDR and the tropics as a whole. All three indices are calculated for the hurricane season in the North Atlantic, which is June–November (JJASON). An increase in MDR precipitation, inverse vertical zonal-wind shear, or the relative SST indicates an increase in TC frequency.

We find that all three TC indices show reduction in TC frequency under SSP2-4.5 (Fig. 13), in agreement with the existing literature (Bengtsson et al., 2007; Knutson et al., 2010; Camargo, 2013). TC frequency also decreases with SAI deployment, but the magnitude of reduction in TC frequency under different SAI strategies varies among the different TC metrics. In general, lower-latitude injections tend to have a larger reduction in the average MDR precipitation (Fig. A2), which yields a larger reduction in TC frequency compared to SSP2-4.5 or the higher-latitude injections (Fig. 13(a)). However, Fig. 13(b) shows that lower-latitude injections result in less increase in the zonal wind shear, which yields a smaller reduction in TC frequency compared to higher-latitude injections. The relative change in the inverse zonal wind shear between different SAI strategies is generally consistent with the relative change in ITCZ location in JJASON (Fig. A6), as a southward shift of ITCZ is related to an increase in zonal wind shear over the MDR (Dunstone et al., 2013). For the SST-based TC metric, we find that all SAI strategies result in substantially stronger reduction in TC frequency than those caused by climate change alone (Fig. 13(c)). The magnitude of the SST-based TC response in the geoengineering runs is smallest for the 60N+60S SAI strategy.

5 Summary

The question of whether to deploy SAI requires not just one simple answer but a series of deliberate decisions on how much cooling to provide, what other climate objectives to achieve, and how to achieve them. Understanding the differences in surface climate responses between different injection strategies is crucial for making informed decisions.

In this work, we have considered a comprehensive set of SAI strategies under the same climate and SAI scenario to explore the range of possible climate responses. These include four hemispherically-symmetric injection strategies designed to maintain global mean temperature and one multi-objective strategy designed to maintain not only the global mean temperature but also the large-scale horizontal temperature gradients. The four hemispherically-symmetric strategies are SO_2 injection at the equator, and injections of equal SO_2 amounts at 15° N and 15° S, at 30° N and 30° S, and at 60° N and 60° S, the latter only during spring in each hemisphere.

The choice of SAI strategies notably affects the spatiotemporal distribution of aerosol optical depths (AOD) and injection efficiencies, and ultimately various surface climate responses. Injecting SO_2 in the mid-latitudes provides more cooling per unit of injection than injecting in either the tropics or high latitudes. The low efficiency in the equatorial injection is primarily due to larger sizes of aerosols formed. The low efficiency in the high-latitude injection case is due to the aerosols having a much shorter lifetime. On the other hand, the 60N+60S case yields the highest global cooling per unit of global mean AOD.

We find that while all of these five SAI strategies maintain the global mean temperature at the reference level, they also overcompensate the interhemispheric temperature gradient. The amount of reduction in the equator-to-pole temperature gradient depends on the choice of SAI strategy, with the high latitude strategy yielding most reduction. In addition, all strategies overcompensate global mean precipitation except the 60N+60S case. This is because injecting at lower latitudes results in stronger tropical cooling and more stratospheric heating, both of which lead to more reduction in precipitation.

Compared to the SSP2-4.5 case, all SAI strategies effectively reduce the percentage of area with statistically significant changes in temperature relative to the quasi present-day reference period, as well as the area-weighted root mean square (rms) change in regional temperature. In contrast, SAI strategies do not consistently reduce the rms change in precipitation minus evaporation (P-E) over land, nor the rms precipitation changes; the 15N+15S and 60N+60S strategies decrease the rms P-E change over land, while the other strategies slightly increase it.

The results show that while all SAI simulations reduce the weakening of the Atlantic meridional overturning circulation that is otherwise found for SSP2-4.5, they also fail to restore it back to the reference period level. Regarding September Arctic sea ice (SSI), all SAI strategies restore SSI back to the reference period level, except the high-latitude injection strategy, which overcompensates SSI. The responses in the location of intertropical convergence zone and tropical cyclone frequencies vary among different SAI strategies.

6 Discussion

Assessing the possible outcomes of SAI requires a good understanding of the possible impact from both the scenario and the choice of injection strategy. MacMartin et al. (2022) have explored how different scenarios affect the climate responses to the same SAI strategy. In this work, we have demonstrated that different SAI strategies with similar objectives and under the same scenario would also affect the surface climate differently, with different distributions of outcomes. The study of these two different dimensions in the SAI design space lays the foundation for understanding the fundamental limits of SAI. Future research will explore combinations of these strategies, along with additional single-latitude cases (Visioni et al., 2022; Lee et al., 2023), to identify an optimal strategy for a given set of climate goals, and assess the underlying trade-offs between different climate goals. Ultimately, knowing the range of possible climate outcomes and the trade-offs will help make informed decisions on future policy on SAI deployment.

In addition, our study demonstrates that the multi-objective strategy (Kravitz et al., 2017; Tilmes et al., 2018; Richter et al., 2022) yields smaller residual regional temperature response than the hemispherically-symmetric strategies considered here. However, such a strategy requires adjusting injection rates across four different latitudes to manage multiple goals, and can thus be challenging to implement across many climate models. Simpler hemispherically-symmetric strategies would be easier to replicate in a large multi-model intercomparison: either the combined 15N+15S or 30N+30S case considered here may represent a reasonable trade-off between how well a strategy compensates for climate changes, and complexity of implementation in a climate model. Our study thus provides fundamental understanding of the differences in the resulting climate responses between the more complex multi-objective strategy and simpler hemispherically-symmetric ones, and as such is directly important for designing and understanding future large inter-model intercomparisons, including the next (seventh) phase of the Geoengineering Model Intercomparison Project (GeoMIP).

It is important to note that all simulations considered here are conducted using a single climate model, namely CESM2(WACCM6). Different climate models yield different patterns of AOD and surface climate responses for the same injection strategy (Visioni et al., 2022; Fasullo and Richter, 2023). Also, atmospheric and climate responses from strategies with different injection locations are subject to different model structural uncertainties (e.g., Visioni et al., 2023; Bednarz et al., 2023). Simulating the same set of injection strategies in different global climate models will thus be important for better characterizing the uncertainties. In addition, the current study uses only a limited number of climate metrics to compare the different SAI strategies, and other aspects of climate that are not analyzed here (i.e. Antarctic ice sheets, permafrost carbon, sea level, ozone, etc), may provide additional insights on the benefits and risks of SAI.

Data availability. Data for the new simulations presented in this study are available at https://doi.org/10.5281/zenodo.7545452 (Zhang et al., 2023). Data for multi-objective strategy (from Visioni, 2022) are available at https://doi.org/10.7298/xr82-sv86.

Appendix A

A1 Hydrological sensitivity

To understand what factors affect the overcompensation of global mean precipitation, we use the precipitation and temperature data from the five SAI strategies as well as SSP2-4.5 to calculate the hydrological sensitivity under different SAI strategies.

The results in Fig. A1 show that the hydrological sensitivity has a strong dependence on the injection latitude; injecting SO_2 at lower latitudes yields a stronger reduction of global mean precipitation per unit of global mean temperature (Fig. A1(a)). EQ has the strongest reduction in precipitation per unit of cooling, followed by 15N+15S, multi-objective, and 30N+30S; the 60N+60S strategy has the least reduction in precipitation per unit of cooling. This dependence on the injection latitude is also observed in the tropical region: injecting at lower latitudes yields a stronger reduction of tropical mean precipitation per unit of tropical mean temperature (Fig. A1(b)), and so it follows that the injection latitude dependence of the global mean precipitation response is not just the result of how much tropical cooling does a given SAI strategy achieves. In fact, the change in precipitation per unit of cooling is larger in the tropics than on the global level. In that case, the dependence on latitude is likely due to the differences in the magnitude of aerosol-induced lower stratospheric heating. Lower latitude injections yield more stratospheric heating. An increase in lower stratospheric temperatures increases the static stability of the troposphere and, thus, reduces tropospheric convection. An increase in tropospheric static stability results in a larger reduction in precipitation. As a result, EQ has the largest reduction in precipitation per unit of cooling and 60N+60S has the smallest reduction in precipitation per unit of cooling. Because adding aerosols to the stratosphere leads to stratospheric heating, the reduction of precipitation under SAI forcing is always larger than the reduction of precipitation by lowering CO_2 concentration in the troposphere.

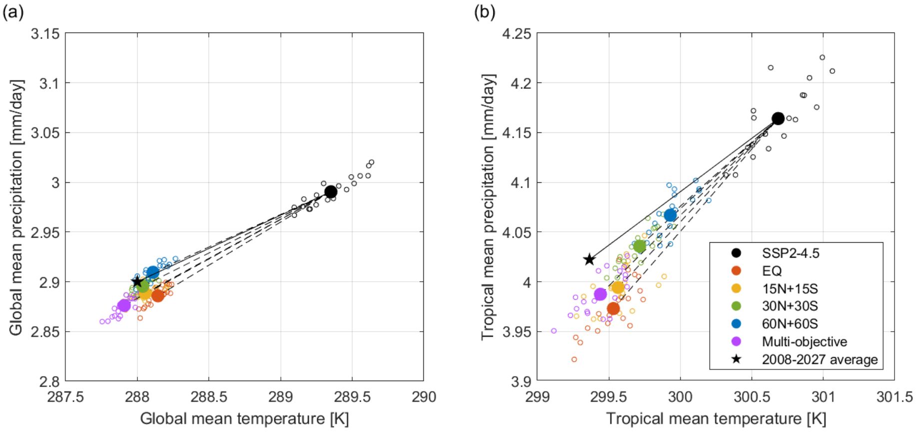

Figure A1. A comparison (a) between the global mean temperature and global mean precipitation, and (b) between the tropical mean temperature and tropical mean precipitation. The tropical means are calculated over the region between 20° N and 20° S. All data shown here are ensemble means. Small hollow dots represent the annual means from 2050–2069 under SSP2-4.5 or a given SAI strategy, and large solid dots represent the 20-year average over 2050–2069. The black star represents the 20-year average of temperature and precipitation from the reference period (2008–2027). The dashed lines show the trajectory of changes in precipitation and temperature under different SAI strategies. The slope of dashed lines indicates the precipitation reduction per unit of cooling under SAI forcing. Similarly, the solid line shows the trajectory of changes in precipitation and temperature under SSP2-4.5. The slope of the solid line represents the increase in precipitation per unit of warming under climate change. The slope in (a) is also called the hydrological sensitivity. These trajectories show a strong dependence on injection latitude; injecting at lower latitudes yields a stronger reduction of global mean precipitation per unit of global cooling and a stronger reduction of tropical mean precipitation per unit of tropical cooling.

A2 Regional precipitation response

Under the SSP2-4.5 scenario, about 43 % of the area has a statistically significant change in precipitation compared to the reference period (2008–2027). None of the SAI strategies fully compensates for the regional precipitation changes under SSP2-4.5. While the percentage of area with statistically significant change in precipitation (27–38 %) is slightly reduced by 445 SAI, SSP2-4.5 and SAI scenarios share similar spatial patterns of changes in precipitation. In particular, among SSP2-4.5 and all SAI cases, the most significant change occurs in the equatorial Pacific Ocean and follows a similar pattern – i.e. precipitation decreases in the northern region and increases in the southern region. This corresponds to the ITCZ shifts discussed in Section 4.4, and the fact that none of the SAI strategies manage to fully offset the southward ITCZ shift simulated in SSP2-4.5.

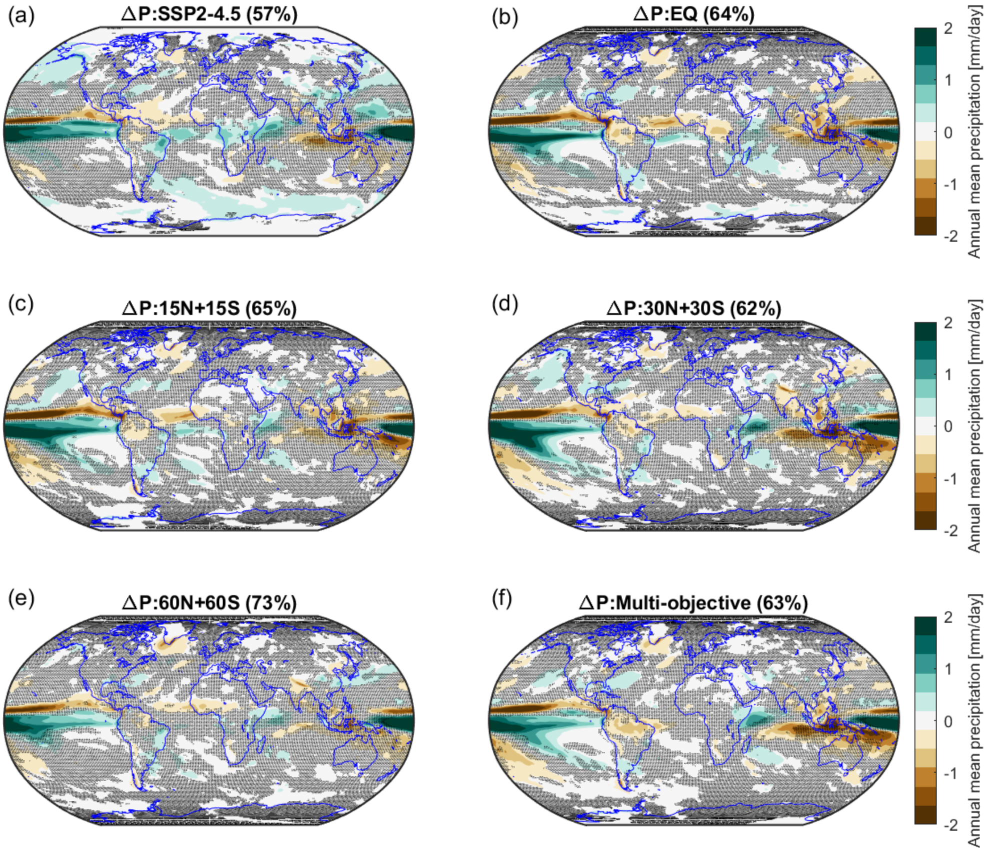

Figure A2. Changes in precipitation averaged over 2050–2069, compared to the reference period (2008–2027) for (a) SSP2-4.5 and (b)-(f) different SAI injection strategies. Shaded areas indicate where the response is not statistically significant based on a two-tailed Welch's t-test with a confidence level of 95 %. The percentage of area with no statistically significant change in precipitation is listed in the title of each map.

https://doi.org/10.5194/egusphere-2023-117
Preprint. Discussion started: 2 March 2023

A3 Additional plots of surface climate responses

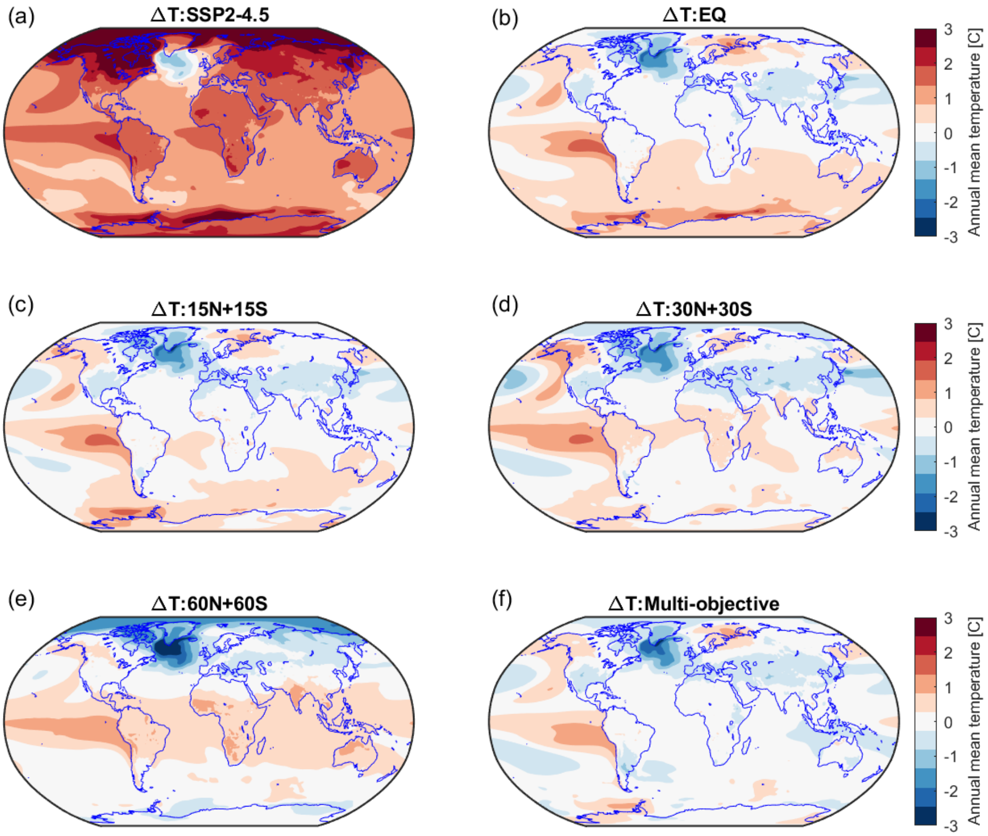

Figure A3. Changes in surface air temperature, averaged over 2050–2069, compared to the reference period (2008–2027) for (a) SSP2-4.5 and (b)-(f) different SAI injection strategies. The plots are as in Fig. 7, but with Welch's t-test results removed for clarity.

https://doi.org/10.5194/egusphere-2023-117
Preprint. Discussion started: 2 March 2023

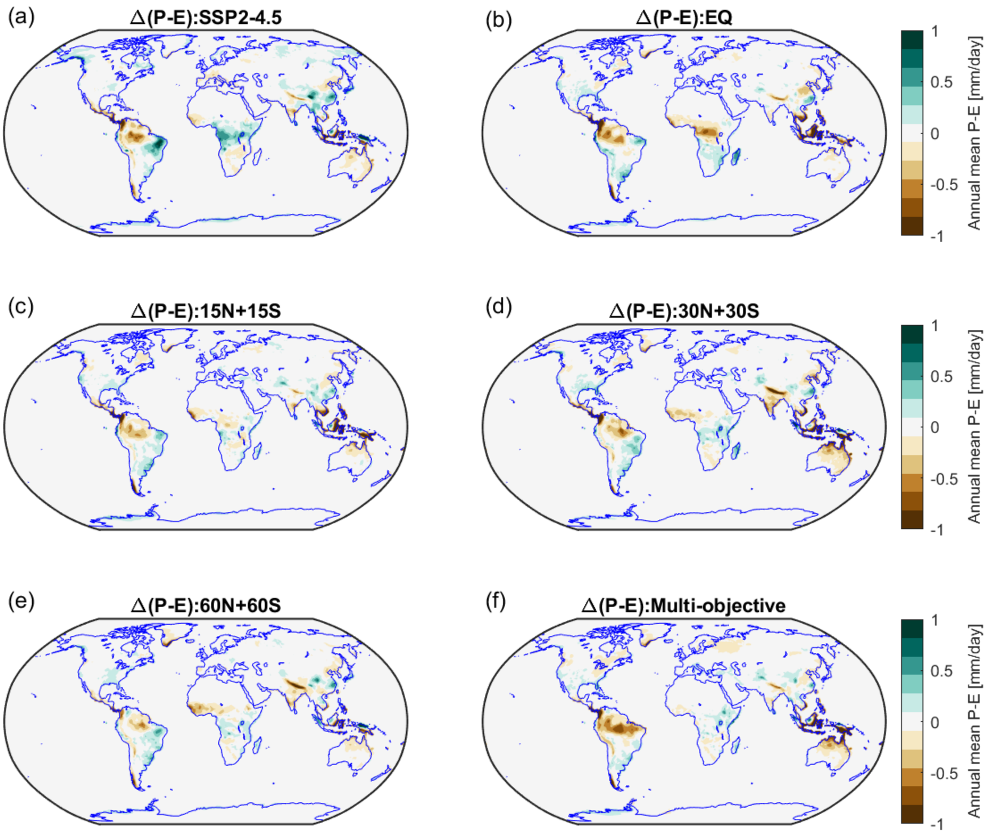

Figure A4. Changes in precipitation minus evaporation (P-E) over land, averaged over 2050–2069, compared to the reference period (2008–2027) for (a) SSP2-4.5 and (b)-(f) different SAI injection strategies. The plots are as in Fig. 9, but with Welch's t-test results removed for clarity.

https://doi.org/10.5194/egusphere-2023-117
Preprint. Discussion started: 2 March 2023

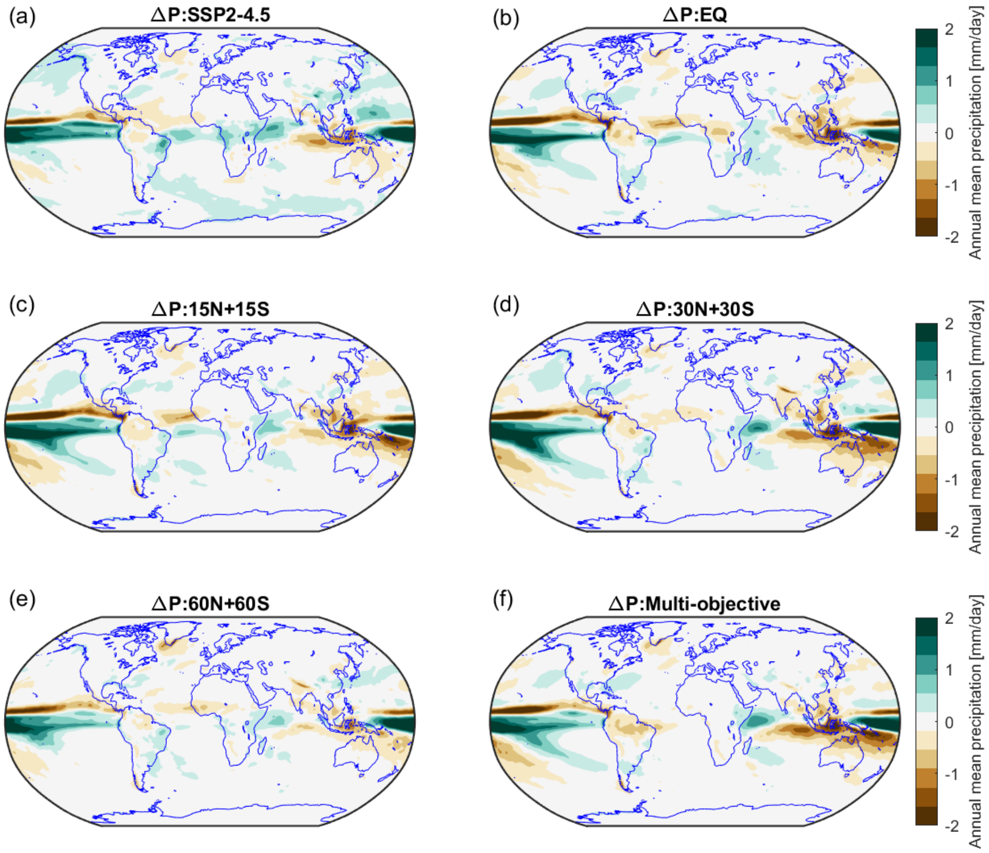

Figure A5. Changes in precipitation, averaged over 2050–2069, compared to the reference period (2008–2027) for (a) SSP2-4.5 and (b)-(f) different SAI injection strategies. The plots are as in Fig. A2, but with Welch's t-test results removed for clarity.

450 ## A4 Additional plot for intertropical convergence zone (ITCZ)

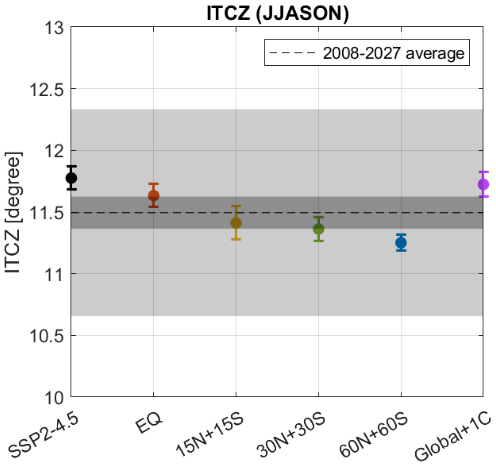

Figure A6. The 20-year (2050–2069) average (dots) and standard error (vertical bars) of the mean latitude of ITCZ averaged over June-November (JJASON) for SSP2-4.5 and the different SAI strategies. The dashed horizontal line represents the mean latitude of ITCZ during the reference period (2008–2027) and the shaded areas represent the corresponding standard error (dark gray) and standard deviation (light gray).

Author contributions. YZ conducted all analyses and wrote the paper with editing from DM, EB, DV and BK; YZ and DM conceived the study with input from all authors and EB and DV assisted with conducting simulations.

Competing interests. The authors declare that they have no conflict of interest.

Acknowledgements. The authors would like to acknowledge high-performance computing support from Cheyenne (https://doi.org/10.5065/D6RX99HX) 455 provided by NCAR's Computational and Information Systems Laboratory, sponsored by the National Science Foundation. Support for Y. Zhang and D. G. MacMartin was provided by the National Science Foundation through agreement CBET-2038246. Support for D. Visioni and E.M. Bednarz was provided by the Cornell Atkinson Center for a Sustainable Future. Support for BK was provided in part by the National Science Foundation through agreement CBET-1931641, the Indiana University Environmental Resilience Institute, and the Prepared for Environmental Change Grand Challenge initiative. The Pacific Northwest National Laboratory is operated for the U.S. Department of Energy by Battelle Memorial Institute under contract DEAC05-76RL01830. The CESM project is supported primarily by the National Science Foundation.

References

Allen, M. R. and Ingram, W. J.: Constraints on future changes in climate and the hydrological cycle, Nature, 419, 223–232, 2002.

Anderson, K., Broderick, J., and Stoddard, I.: A factor of two: how the mitigation plans of 'climate progressive' nations fall far short of Paris-compliant pathways, Clim. Policy, 20, 1290–1304, https://doi.org/10.1080/14693062.2020.1728209, 2020.

Bala, G., Duffy, P. B., and Taylor, K. E.: Impact of geoengineering schemes on the global hydrological cycle, PNAS, 105, 7664–7669, 2008.

Bala, G., Caldeira, K., and Nemani, R.: Fast versus slow response in climate change: implications for the global hydrological cycle, Clim. Dyn., 35, 423–434, doi:10.1007/s00382-009-0583-y, 2010.

Bamber, J. L., Oppenheimer, M., Kopp, R. E., Aspinall, W., and Cooke, R.: Ice sheet contributions to future sea-level rise from structured expert judgment, PNAS, 116, 11 195–11 200, https://doi.org/10.1073/pnas.1817205116, 2019.

Bednarz, E. M., Visioni, D., Kravitz, B., Jones, A., Haywood, J. M., Richter, J., MacMartin, D. G., and Braesicke, P.: Climate response to off-equatorial stratospheric sulfur injections in three Earth System Models – Part 2: stratospheric and free-tropospheric response, Atmospheric Chemistry and Physics Discussions, 2022, 1–30, https://doi.org/10.5194/acp-2022-372, 2022a.

Bednarz, E. M., Visioni, D., Richter, J. H., Butler, A. H., and MacMartin, D. G.: Impact of the Latitude of Stratospheric Aerosol Injection on the Southern Annular Mode, Geophysical Research Letters, 49, e2022GL100 353, https://doi.org/10.1029/2022GL100353, e2022GL100353 2022GL100353, 2022b.

Bednarz, E. M., Visioni, D., Kravitz, B., Jones, A., Haywood, J. M., Richter, J., MacMartin, D. G., and Braesicke, P.: Climate response to off-equatorial stratospheric sulfur injections in three Earth system models – Part 2: Stratospheric and free-tropospheric response, Atmospheric Chemistry and Physics, 23, 687–709, https://doi.org/10.5194/acp-23-687-2023, 2023.

Bengtsson, L., Hodges, K. I., and Esch, M.: Tropical cyclones in a T159 resolution global climate model: comparison with observations and re-analyses, Tellus A, 59, 396–416, https://doi.org/https://doi.org/10.1111/j.1600-0870.2007.00236.x, 2007.

Bjordal, J., Trude, S., Alterskjær, K., and Carlsen, T.: Equilibrium climate sensitivity above 5 °C plausible due to state-dependent cloud feedback, Nature Geoscience, 13, 718–721, https://doi.org/10.1038/s41561-020-00649-1, 2020.

Burgess, M. G., Ritchie, J., Shapland, J., and Pielke, R.: IPCC baseline scenarios have over-projected CO2 emissions and economic growth, Environ. Res. Lett., 16, 014 016, https://doi.org/10.1088/1748-9326/abcdd2, 2021.

Butchart, N.: The Brewer-Dobson circulation, Reviews of Geophysics, 52, 157–184, https://doi.org/https://doi.org/10.1002/2013RG000448, 2014.

Byrne, M., Pendergrass, A., Rapp, A., and Wodzicki, K.: Response of the Intertropical Convergence Zone to Climate Change: Location, Width, and Strength, Current Climate Change Reports, 4, 355–370, https://doi.org/10.1007/s40641-018-0110-5, 2018.

Camargo, S. J.: Global and Regional Aspects of Tropical Cyclone Activity in the CMIP5 Models, Journal of Climate, 26, 9880 – 9902, https://doi.org/10.1175/JCLI-D-12-00549.1, 2013.

Chemke, R., Zanna, L., and Polvani, L. M.: Identifying a human signal in the North Atlantic warming hole, Nature Communications, 11, 1540, https://doi.org/10.1038/s41467-020-15285-x, 2020.

Cheng, W., MacMartin, D. G., Kravitz, B.and Visioni, D., Bednarz, E. M., Xu, Y., Luo, Y., Huang, L., Hu, Y., Staten, P. W., Hitchcock, P., Moore, J. C., Guo, A., and Deng, X.: Changes in Hadley circulation and intertropical convergence zone under strategic stratospheric aerosol geoengineering, npj Climate and Atmospheric Science, 5, 32, https://doi.org/10.1038/s41612-022-00254-6, 2022.

Danabasoglu, G.: On Multidecadal Variability of the Atlantic Meridional Overturning Circulation in the Community Climate System Model Version 3, Journal of Climate, 21, 5524–5544, https://doi.org/10.1175/2008JCLI2019.1, 2008.

Danabasoglu, G., Lamarque, J.-F., Bacmeister, J., Bailey, D. A., DuVivier, A. K., Edwards, J., Emmons, L. K., Fasullo, J., Garcia, R., Gettelman, A., Hannay, C., Holland, M. M., Large, W. G., Lauritzen, P. H., Lawrence, D. M., Lenaerts, J. T. M., Lindsay, K., Lipscomb, W. H., Mills, M. J., Neale, R., Oleson, K. W., Otto-Bliesner, B., Phillips, A. S., Sacks, W., Tilmes, S., van Kampenhout, L., Vertenstein, M., Bertini, A., Dennis, J., Deser, C., Fischer, C., Fox-Kemper, B., Kay, J. E., Kinnison, D., Kushner, P. J., Larson, V. E., Long, M. C., Mickelson, S., Moore, J. K., Nienhouse, E., Polvani, L., Rasch, P. J., and Strand, W. G.: The Community Earth System Model Version 2 (CESM2), Journal of Advances in Modeling Earth Systems, 12, e2019MS001 916, https://doi.org/https://doi.org/10.1029/2019MS001916, e2019MS001916 2019MS001916, 2020.

Davis, N. A., Visioni, D., Garcia, R. R., Kinnison, D. E., Marsh, D. R., Mills, M. J., Richter, J. H., Tilmes, S., Bardeen, C., Gettelman, A., Glanville, A. A., MacMartin, D. G., Smith, A. K., and Vitt, F.: Climate, variability, and climate sensitivity of “Middle Atmosphere” chemistry configurations of the Community Earth System Model Version 2, Whole Atmosphere Community Climate Model Version 6 (CESM2(WACCM6)), https://doi.org/10.22541/essoar.167117634.40175082/v1, 2022.

Donohoe, A., Marshall, J., Ferreira, D., and Mcgee, D.: The Relationship between ITCZ Location and Cross-Equatorial Atmospheric Heat Transport: From the Seasonal Cycle to the Last Glacial Maximum, Journal of Climate, 26, 3597 – 3618, https://doi.org/10.1175/JCLI-D-12-00467.1, 2013.

Dunstone, N., Smith, D., Booth, B., Hermanson, L., and Eade, R.: Anthropogenic aerosol forcing of Atlantic tropical storms, Nature Geoscience, 6, 534–539, https://doi.org/10.1038/ngeo1854, 2013.

Dvorak, M. T., Armour, K. C., Frierson, D. M. W., Proistosescu, C., Baker, M. B., and Smith, C. J.: Estimating the timing of geophysical commitment to 1.5 and 2.0 °C of global warming, Nature Climate Change, 12, 547–552, https://doi.org/10.1038/s41558-022-01372-y, 2022.

Fasullo, J. T. and Richter, J. H.: Dependence of strategic solar climate intervention on background scenario and model physics, Atmospheric Chemistry and Physics, 23, 163–182, https://doi.org/10.5194/acp-23-163-2023, 2023.

Frierson, D. M. W. and Hwang, Y.-T.: Extratropical Influence on ITCZ Shifts in Slab Ocean Simulations of Global Warming, Journal of Climate, 25, 720 – 733, https://doi.org/10.1175/JCLI-D-11-00116.1, 2012.

Gettelman, A., Mills, M. J., Kinnison, D. E., Garcia, R. R., Smith, A. K., Marsh, D. R., Tilmes, S., Vitt, F., Bardeen, C. G., McInerny, J., Liu, H.-L., Solomon, S. C., Polvani, L. M., Emmons, L. K., Lamarque, J.-F., Richter, J. H., Glanville, A. S., Bacmeister, J. T., Phillips, A. S., Neale, R. B., Simpson, I. R., DuVivier, A. K., Hodzic, A., and Randel, W. J.: The Whole Atmosphere Community Climate Model Version 6 (WACCM6), Journal of Geophysical Research: Atmospheres, 124, 12 380–12 403, https://doi.org/https://doi.org/10.1029/2019JD030943, 2019.

Guo, A., Moore, J. C., and Ji, D.: Tropical atmospheric circulation response to the G1 sunshade geoengineering radiative forcing experiment, Atmospheric Chemistry and Physics, 18, 8689–8706, https://doi.org/10.5194/acp-18-8689-2018, 2018.

Hahn, L. C., Armour, K. C., Zelinka, M. D., Bitz, C. M., and Donohoe, A.: Contributions to Polar Amplification in CMIP5 and CMIP6 Models, Frontiers in Earth Science, 9, https://doi.org/10.3389/feart.2021.710036, 2021.

Hari, V., Villarini, G., Karmakar, S., Wilcox, L. J., and Collins, M.: Northward Propagation of the Intertropical Convergence Zone and Strengthening of Indian Summer Monsoon Rainfall, Geophysical Research Letters, 47, e2020GL089 823, https://doi.org/https://doi.org/10.1029/2020GL089823, e2020GL089823 2020GL089823, 2020.

Holland, M. M. and Bitz, C. M.: Polar amplification of climate change in coupled models, Climate Dynamics, 21, 221–232, https://doi.org/10.1007/s00382-003-0332-6, 2003.

IPCC: Climate Change 2021: The Physical Science Basis. Contribution of Working Group I to the Sixth Assessment Report of the Intergovernmental Panel on Climate Change, https://doi.org/10.1017/9781009157896, in Press, 2021.

Irvine, P., Emanuel, K., He, J., Horowitz, L. W., Vecchi, G., and Keith, D.: Halving warming with idealized solar geoengineering moderates key climate hazards, Nature Climate Change, 9, 295–299, 2019.

Jones, A., Haywood, J., Dunstone, N., et al.: Impacts of hemispheric solar geoengineering on tropical cyclone frequency, Nat. commun., 8, 1382, https://doi.org/10.1038/s41467-017-01606-0, 2017.

Keil, P. et al.: Multiple drivers of the North Atlantic warming hole, Nature Climate Change, 10, 667–671, https://doi.org/10.1038/s41558-020-0819-8, 2020.

Kleinschmitt, C., Boucher, O., and Platt, U.: Sensitivity of the radiative forcing by stratospheric sulfur geoengineering to the amount and strategy of the SO_2 injection studied with the LMDZ-S3A model, Atmos. Chem. Phys., 18, 2769–2786, doi:10.5194/acp-18-2769-2018, 2018.

Knutson, T., McBride, J., Chan, J., et al.: Tropical cyclones and climate change, Nature Geoscience, 3, 1752–0908, https://doi.org/10.1038/ngeo779, 2010.

Kravitz, B., MacMartin, D. G., Wang, H., and Rasch, P. J.: Geoengineering as a Design Problem, Earth Systems Dynamics, 7, 469–497, doi:10.5194/esd-7-469-2016, 2016.

Kravitz, B., MacMartin, D. G., Mills, M. J., Richter, J. H., Tilmes, S., Lamarque, J.-F., Tribbia, J. J., and Vitt, F.: First simulations of designing stratospheric sulfate aerosol geoengineering to meet multiple simultaneous climate objectives, J. Geophys. Res. A, 122, 12,616–12,634, doi:10.1002/2017JD026874, 2017.

Kravitz, B. et al.: Comparing surface and stratospheric impacts of geoengineering with different SO_2 injection strategies, J. Geophys. Res. A, 124, 2019.

Lee, W., MacMartin, D., Visioni, D., and Kravitz, B.: Expanding the design space of stratospheric aerosol geoengineering to include precipitation-based objectives and explore trade-offs, Earth System Dynamics, 11, 1051–1072, https://doi.org/10.5194/esd-11-1051-2020, 2020.

Lee, W., MacMartin, D., Visioni, D., and Kravitz, B.: High-Latitude stratospheric aerosol geoengineering can be more effective if injection is limited to spring, Geophysical Research Letters, 48, https://doi.org/10.1029/2021GL092696, 2021.

Lee, W. R., MacMartin, D. G., Visioni, D., Kravitz, B., Chen, Y., Moore, J. C., Leguy, G., Lawrence, D. M., and Bailey, D. A.: High-Latitude Stratospheric Aerosol Injection to Preserve the Arctic, Earth's Future, 11, e2022EF003052, https://doi.org/https://doi.org/10.1029/2022EF003052, 2023.

MacMartin, D. G., Kravitz, B., Keith, D. W., and Jarvis, A. J.: Dynamics of the coupled human-climate system resulting from closed-loop control of solar geoengineering, Clim. Dyn., 43, 243–258, 2014.

MacMartin, D. G., Kravitz, B., Tilmes, S., Richter, J. H., Mills, M. J., Lamarque, J.-F., Tribbia, J. J., and Vitt, F.: The climate response to stratospheric aerosol geoengineering can be tailored using multiple injection locations, J. Geophys. Res. A, 122, 12,574–12,590, doi:10.1002/2017JD026868, 2017.

MacMartin, D. G., Wang, W., Kravitz, B., Tilmes, S., Richter, J., and Mills, M. J.: Timescale for detecting the climate response to stratospheric aerosol geoengineering, J. Geophys. Res. A, 124, 2019.

MacMartin, D. G., Visioni, D., Kravitz, B., Richter, J., Felgenhauer, T., Lee, W. R., Morrow, D. R., Parson, E. A., and Sugiyama, M.: Scenarios for modeling solar radiation modification, Proceedings of the National Academy of Sciences, 119, e2202230119, https://doi.org/10.1073/pnas.2202230119, 2022.

McGregor, S., Cassou, C., Kosaka, Y., and Phillips, A. S.: Projected ENSO Teleconnection Changes in CMIP6, Geophysical Research Letters, 49, e2021GL097 511, https://doi.org/https://doi.org/10.1029/2021GL097511, e2021GL097511 2021GL097511, 2022.

Meinshausen, M., Nicholls, Z. R. J., Lewis, J., Gidden, M. J., Vogel, E., Freund, M., Beyerle, U., Gessner, C., Nauels, A., Bauer, N., Canadell, J. G., Daniel, J. S., John, A., Krummel, P. B., Luderer, G., Meinshausen, N., Montzka, S. A., Rayner, P. J., Reimann, S., Smith, S. J., van den Berg, M., Velders, G. J. M., Vollmer, M. K., and Wang, R. H. J.: The shared socio-economic pathway (SSP) greenhouse gas concentrations and their extensions to 2500, Geoscientific Model Development, 13, 3571–3605, https://doi.org/10.5194/gmd-13-3571-2020, 2020.

Meinshausen, M., Lewis, J., McGlade, C., Gütschow, J., Nicholls, Z., et al.: Realization of Paris Agreement pledges may limit warming just below 2 °C, Nature, 604, 304–309, https://doi.org/10.1038/s41586-022-04553-z, 2022.

Mills, M., Richter, J. H., Tilmes, S., Kravitz, B., MacMartin, D. G., Glanville, A. A., Tribbia, J. J., Lamarque, J.-F., Vitt, F., Schmidt, A., Gettelman, A., Hannay, C., Bacmeister, J. T., and Kinnison, D. E.: Radiative and chemical response to interactive stratospheric aerosols in fully coupled CESM1(WACCM), J. Geophys. Res. A., 122, 13,061–13,078, doi:10.1002/2017JD027006, 2017.

Niemeier, U. and Timmreck, C.: What is the limit of climate engineering by stratospheric injection of SO_2?, Atmos. Chem. Phys., 15, 9129–9141, 2015.

Niemeier, U., Schmidt, H., Alterskjær, K., and Kristjánsson, J. E.: Solar irradiance reduction via climate engineering: Impact of different techniques on the energy balance and the hydrological cycle, J. Geophys. Res.: Atmospheres, 118, 11,905–11,917, doi:10.1002/2013JD020445, 2013.

Notz, D. and Stroeve, J.: The Trajectory Towards a Seasonally Ice-Free Arctic Ocean, Current Climate Change Reports, 4, 407–416, https://doi.org/10.1007/s40641-018-0113-2, 2018.

O'Gorman, P. A., Allan, R. P., Byrne, M. P., and Previdi, M.: Energetic Constraints on Precipitation Under Climate Change, Surveys in Geophysics, 33, 585–608, https://doi.org/10.1007/s10712-011-9159-6, 2012.

Previdi, M., Smith, K. L., and Polvani, L. M.: Arctic amplification of climate change: a review of underlying mechanisms, Environmental Research Letters, 16, 093 003, https://doi.org/10.1088/1748-9326/ac1c29, 2021.

Rahmstorf, S.: Ocean circulation and climate during the past 120,000 years, Nature, 419, 207–214, https://doi.org/10.1038/nature01090, 2002.

Richter, J., Visioni, D., MacMartin, D., Bailey, D., Rosenbloom, N., Lee, W., Tye, M., and Lamarque, J.-F.: Assessing Responses and Impacts of Solar climate intervention on the Earth system with stratospheric aerosol injection (ARISE-SAI), EGUsphere, 2022, 1–35, https://doi.org/10.5194/egusphere-2022-125, 2022.

Rogelj, J., den Elzen, M., Höhne, N., Fransen, T., Fekete, H., Winkler, H., Schaeffer, R., Sha, F., Riaha, K., and Meinshausen, M.: Paris Agreement climate proposals need a boost to keep warming well below 2°C, Nature, 534, 631–639, doi:10.1038/nature18307, 2016.

Serreze, M. and Barry, R.: Processes and impacts of Arctic amplification: A research synthesis, Global and Planetary Change, 77, 85–96, https://doi.org/10.1016/j.gloplacha.2011.03.004, 2011.

Sherwood, S. C., Webb, M. J., Annan, J. D., Armour, K. C., Forster, P. M., Hargreaves, J. C., Hegerl, G., Klein, S. A., Marvel, K. D., Rohling, E. J., Watanabe, M., Andrews, T., Braconnot, P., Bretherton, C. S., Foster, G. L., Hausfather, Z., von der Heydt, A. S., Knutti, R., Mauritsen, T., Norris, J. R., Proistosescu, C., Rugenstein, M., Schmidt, G. A., Tokarska, K. B., and Zelinka, M. D.: An Assessment of Earth's Climate Sensitivity Using Multiple Lines of Evidence, Reviews of Geophysics, 58, e2019RG000 678, https://doi.org/https://doi.org/10.1029/2019RG000678, e2019RG000678 2019RG000678, 2020.

Simpson, I. R., Tilmes, S., Richter, J. H., Kravitz, B., MacMartin, D. G., Mills, M. J., Fasullo, J. T., and Pendergrass, A. G.: The Regional Hydroclimate Response to Stratospheric Sulfate Geoengineering and the Role of Stratospheric Heating, Journal of Geophysical Research: Atmospheres, 124, 12 587–12 616, https://doi.org/10.1029/2019JD031093, 2019.

Tebaldi, C., Debeire, K., Eyring, V., Fischer, E., Fyfe, J., Friedlingstein, P., Knutti, R., Lowe, J., O'Neill, B., Sanderson, B., van Vuuren, D., Riahi, K., Meinshausen, M., Nicholls, Z., Tokarska, K. B., Hurtt, G., Kriegler, E., Lamarque, J.-F., Meehl, G., Moss, R., Bauer, S. E., Boucher, O., Brovkin, V., Byun, Y.-H., Dix, M., Gualdi, S., Guo, H., John, J. G., Kharin, S., Kim, Y., Koshiro, T., Ma, L., Olivié, D., Panickal, S., Qiao, F., Rong, X., Rosenbloom, N., Schupfner, M., Séférian, R., Sellar, A., Semmler, T., Shi, X., Song, Z., Steger, C., Stouffer, R., Swart, N., Tachiiri, K., Tang, Q., Tatebe, H., Voldoire, A., Volodin, E., Wyser, K., Xin, X., Yang, S., Yu, Y., and Ziehn, T.: Climate model projections from the Scenario Model Intercomparison Project (ScenarioMIP) of CMIP6, Earth System Dynamics, 12, 253–293, https://doi.org/10.5194/esd-12-253-2021, 2021.

Tilmes, S., Richter, J. H., Mills, M. J., Kravitz, B., MacMartin, D. G., Vitt, F., Tribbia, J. J., and Lamarque, J.-F.: Sensitivity of aerosol distribution and climate response to stratospheric SO_2 injection locations, J. Geophys. Res. A., 122, 12,591–12,615, doi:10.1002/2017JD026888, 2017.

Tilmes, S., Richter, J. H., Kravitz, B., MacMartin, D. G., Mills, M. J., Simpson, I., Glanville, A. S., Fasullo, J. T., Phillips, A. S., Lamarque, J.-F., Tribbia, J., Edwards, J., Mickelson, S., and Gosh, S.: CESM1(WACCM) stratospheric aerosol geoengineering large ensemble (GLENS) project, Bull. Am. Met. Soc., doi:10.1175/BAMS-D-17-0267.1, 2018.

Tilmes, S. et al.: The hydrological impact of geoengineering in the Geoengineering Model Intercomparison Project (GeoMIP), J. Geophys. Res., 118, 11 036–11 058, doi:10.1002/jgrd.50868, 2013.

Tilmes, S. et al.: Reaching 1.5°C and 2.0°C global surface temperature targets using stratospheric aerosol geoengineering in CMIP6, submitted, Earth Sys. Dyn., 2020.

UNEP: Emissions Gap Report 2021: The Heat Is On – A World of Climate Promises Not Yet Delivered, https://wedocs.unep.org/20.500.11822/36990, 2021-10.

UNFCCC: Adoption of the Paris Agreement, Available at `https://unfccc.int/resource/docs/2015/cop21/eng/l09.pdf`, 2015.

Visioni, D.: Data from: Scenarios for modeling solar radiation modification [Data set], Cornell University eCommons Repository, https://doi.org/10.7298/xr82-sv86, 2022.

Visioni, D., Pitari, G., Aquila, V., Tilmes, S., Cionni, I., Di Genova, G., and Mancini, E.: Sulfate geoengineering impact on methane transport and lifetime: results from the Geoengineering Model Intercomparison Project (GeoMIP), Atmospheric Chemistry and Physics, 17, 11 209–11 226, https://doi.org/10.5194/acp-17-11209-2017, 2017.

Visioni, D., MacMartin, D. G., Kravitz, B., Lee, W., Simpson, I. R., and Richter, J. H.: Reduced Poleward Transport Due to Stratospheric Heating Under Stratospheric Aerosols Geoengineering, Geophysical Research Letters, 47, e2020GL089 470, https://doi.org/10.1029/2020GL089470, 2020a.

Visioni, D., MacMartin, D. G., Kravitz, B., Richter, J. H., Tilmes, S., and Mills, M. J.: Seasonally Modulated Stratospheric Aerosol Geoengineering Alters the Climate Outcomes, Geophysical Research Letters, 47, e2020GL088 337, https://doi.org/10.1029/2020GL088337, 2020b.

Visioni, D., MacMartin, D. G., Kravitz, B., Boucher, O., Jones, A., Lurton, T., Martine, M., Mills, M. J., Nabat, P., Niemeier, U., Séférian, R., and Tilmes, S.: Identifying the sources of uncertainty in climate model simulations of solar radiation modification with the G6sulfur and

G6solar Geoengineering Model Intercomparison Project (GeoMIP) simulations, Atmospheric Chemistry and Physics, 21, 10 039–10 063, https://doi.org/10.5194/acp-21-10039-2021, 2021.

Visioni, D., Bednarz, E. M., Lee, W. R., Kravitz, B., Jones, A., Haywood, J. M., and MacMartin, D. G.: Climate response to off-equatorial stratospheric sulfur injections in three Earth System Models – Part 1: experimental protocols and surface changes, EGUsphere, 2022, 1–34, https://doi.org/10.5194/egusphere-2022-401, 2022.

Visioni, D., Bednarz, E. M., Lee, W. R., Kravitz, B., Jones, A., Haywood, J. M., and MacMartin, D. G.: Climate response to off-equatorial stratospheric sulfur injections in three Earth system models – Part 1: Experimental protocols and surface changes, Atmospheric Chemistry and Physics, 23, 663–685, https://doi.org/10.5194/acp-23-663-2023, 2023.

Wilks, D. S.: Statistical methods in the atmospheric sciences, Elsevier, 2019.

Zhang, Y., MacMartin, D. G., Visioni, D., and Kravitz, B.: How large is the design space for stratospheric aerosol geoengineering?, Earth System Dynamics, 13, 201–217, https://doi.org/10.5194/esd-13-201-2022, 2022.

Zhang, Y., MacMartin, D. G., Visioni, D., Bednarz, E., and Kravitz, B.: Data from: Introducing a Comprehensive Set of Stratospheric Aerosol Injection Strategies [Data set], Zenodo, https://doi.org/10.5281/zenodo.7545452, 2023.

Zhao, M., Cao, L., Bala, G., and Duan, L.: Climate Response to Latitudinal and Altitudinal Distribution of Stratospheric Sulfate Aerosols, Journal of Geophysical Research: Atmospheres, 126, e2021JD035 379, https://doi.org/https://doi.org/10.1029/2021JD035379, e2021JD035379 2021JD035379, 2021.